Elsevier Editorial System(tm) for Solar Energy

Manuscript Draft

Manuscript Number: SE-D-20-01506R1

Title: Silver nanofluids based broadband solar absorber through tuning nanosilver geometries

Article Type: Research paper

Section/Category: Solar heating & cooling, buildings, and other applications

Keywords: Nanofluids; Plasmonic; Broadband solar absorber; Stability; Silver nanoprisms; Silver nanodiscs

Corresponding Author: Professor Xunli Zhang,

Corresponding Author's Institution: University of Southampton

First Author: Harriet Kimpton

Order of Authors: Harriet Kimpton; Eugen Stulz; Xunli Zhang

Abstract: This work explores the strategy for increasing the efficiency of solar thermal energy capture by the utilisation of a blended mixture of plasmonic silver nanofluids in a direct absorption solar collector. For the first time, a broadband absorber based on combining three silver-based nanofluids, each with a tailored plasmonic response covering a different wavelength range, was designed and synthesised. The potential efficiency of this broadband absorber was estimated from the UV-Vis-IR spectra and from direct measurement of the temperature rise obtained in static tests in a solar simulator. The results from the two methods were comparable. The broadband absorber was shown to increase the efficiency of capture compared to the component nanofluids and compared to water. The temperature rise in the solar simulator for the broadband mixture was more than four times that of water and the photo-thermal conversion efficiency was approximately 85%, demonstrating the promise of this mixture for enhancing solar energy capture. However, this work also illustrates the potential issues with utilising silver for solar applications, namely the change in morphology and UV-Vis-IR spectra with light exposure. A suitable stabilisation or coating strategy would hence be required to use this developed broadband absorber in solar energy applications.

Professor Yanjun Dai
Subject Editor
Solar Energy

11 July 2020

Ms. Ref. No.: SE-D-20-01506
Manuscript Title: Silver nanofluids based broadband solar absorber through tuning nanosilver geometries

Dear Professor Dai,

Thank you and the Reviewers for the comments and suggestions provided. Accordingly, we have revised the manuscript, on a point-by-point basis, where the changes are highlighted (in red) throughout the manuscript, which are also summarised below.

We hope the revised manuscript will reach this journal's high-quality standards. Meanwhile, should you require further information about this article, please do not hesitate to contact us any time.

Yours sincerely,

Professor Xunli Zhang
University of Southampton

Reviewer #1: No novelties found.

- To the authors' best knowledge, this is the first attempt to experimentally synthesise and subsequently evaluate a broadband absorber with selected geometries of silver nanoparticles, although the theoretic/numerical concept has been proposed previously, as described in Introduction. (p.4)

Reviewer #2: Authors are required to address the following comments;
1. The statement where the author said; "However, most commonly employed working fluids in DASCs only absorb a low percentage of the solar radiation in the range of 2% to 14% over the wavelength range 200 - 1500 nm (Otanicar et al., 2009)". This statement is no longer valid, this was true only 10 years ago! Currently a lot of studies propose nanofluid with large absorption spectral. Please have a look to the following reference: N Hordy et all 2014.

- The statement was about heat transfer working fluids but not nanofluids, hence is still valid, although now most fluids proposed/studied for DASC are nanofluids. To make it clearer, this sentence has been modified to clarify, as follows.

However, without additions the working fluids employed in most DASCs only absorb a low percentage of the solar radiation in the range of 2% to 14% over the wavelength range 200 - 1500 nm. (p.3)

2. In page 4 authors said; "to the authors' best knowledge, investigations on blended broadband absorbers based on plasmonic silver nanofluids have not been reported."
In my opinion the following numerical work: "Abdul Rahman Mallah , S.N. Kazi, Mohd Nashrul Mohd Zubir, A. Badarudin, Blended morphologies of plasmonic nanofluids for direct absorption applications. Applied Energy Volume 229, 1 November 2018, Pages 505-521, is as innovative as the present manuscript. Please address this comment properly.

- As addressed above about the novelty, to emphasise that this work is primarily experimental and as such differs from the very good numerical study as indicated by the Reviewer, the end of the second paragraph on page 4 has been revised (as follows).

A blended nanofluid has been concepted as the ideal broadband solar absorber for DASC applications (Goel et al., 2020; Sharaf et al., 2019), and two silver broadband mixtures comprising five different silver nanoparticle geometries have been investigated numerically (Mallah et al., 2018). Their two blended nanofluids gave absorption efficiencies of 98 % and 95 % respectively over the range of 300-2500 nm for a nanofluid depth of 10 cm. This work complements this numerical work, using a simpler three component mixture, but provides additional information on issues that occur when mixtures of different nanoparticle geometries are combined together experimentally. The concept of a broadband absorber based on silver is not novel, but to the authors' best knowledge the experimental production and subsequent testing of such a blended broadband absorber mixture has not been reported. (p.4)

- The word "experimental" has been added to the last paragraph on page 4 in Introduction:

"Most experimental studies for DASC applications have focused on nanospheres…"

- More wording has been added to the last paragraph on page 15 to emphasise that additional information is obtained by carrying out experimental rather than numerical studies:

"The cause of the red shift in the secondary λ_{max} is unknown but may be related to the smaller but similar red shift observed on storage for P-B and is additional information which is obtained by carrying out experimental studies."

- More discussion has also been added to the second paragraph on page 22, where the results from this study are compared to other results obtained for blended silver broadband absorbers, as follows.

The numerical study by Mallah et al (Mallah et al., 2018) produced better results for efficiency than this study at a lower concentration but with a longer path length employed (up to 98 % for a 10 cm path length). The absorption obtained in the near IR range was better for the nanofluid they proposed containing silver nanorods. To give a true comparison to this work a five component nanofluid with the same concentrations, nanoparticle types and ratio of components would need to be synthesised and tested using the same geometry as they proposed. In fact in their conclusions they acknowledge the importance of conducting experimental studies on these blended nanofluids.

3. How the optimum combination 50%, 20%, and 30% has been calculated?

- More wording was added to the last paragraph on page 9:

"The $AE_{(300\text{-}1350nm)}$ obtained for various mixtures were calculated using the average UV-Vis-IR spectra for the various components and Equations 1-3 and are given in SI Table S2. The selected calculated combination whilst minimising the amount of P-B (the least stable nanofluid in the mixture) was 50% P-A, 20% P-B and 30% P-C, that equates to 0.247 mM final silver concentration in the mixture. This gave a value of $AE_{(300\text{-}1350nm)}$ of 82.52 % which was slightly lower than the optimum mixture without minimizing P-B of 83.14 % (Table S2)."

- While additional Table and explanation mentioned above have been added to the SI, all subsequent references to Tables in the SI have been checked and renumbered to allow for the addition of the extra Table.
- Further addition to the SI is as follows.

2. Calculation of $AE_{(300\text{-}1350nm)}$ to determine the optimum mixture

The values obtained for the UV-vis-IR spectra for the three repeats of each of the three nanofluids (P-A1, A2, A3, P-B1, B2 and B3 and P-C1, C2 and C3) were averaged and $AE_{(300\text{-}1350nm)}$ for various mixtures calculated. To allow for the dilution of P-B and P-C, the spectra for P-B was times by 3 (diluted 1 ml in 3 ml) and for P-C by 5 (diluted 0.6 ml in 3 ml).

The results are given in *Table S*2.

Table S2 Calculations of optimum mixture. Note although not the optimum in terms of $AE_{(300\text{-}1350nm)}$, the recipe corresponding to calculation 7 was chosen as it minimized the amount of P-B, the least stable nanofluid.

Calculation number	P-A / %	P-B / %	P-C / %	Calculated $AE_{(300\text{-}1350nm)}$ / %	Concentration Ag / mM	Concentration Ag / wt%
1	70	10	20	80.28	0.1914	0.00207
2	70	20	10	80.79	0.1757	0.00190
3	60	10	30	80.93	0.2271	0.00245
4	60	20	20	82.45	0.2114	0.00228
5	60	30	10	82.20	0.1957	0.00211
6	50	10	40	80.33	0.2628	0.00283
7	**50**	**20**	**30**	**82.52**	**0.2471**	**0.00267**
8	50	30	20	83.14	0.2314	0.00250
9	50	40	10	82.61	0.2157	0.00233
10	40	10	50	78.71	0.2985	0.00322
11	40	20	40	81.43	0.2828	0.00305
12	40	30	30	82.63	0.2671	0.00288
13	40	40	20	82.86	0.2514	0.00271
14	40	50	10	82.31	0.2357	0.00254

4. What do you mean by P-A1, P-A2, and P-A3?

- P-A1, P-A2 and P-A3 were defined in the second paragraph of Section 2.2 on page 6. For clarity the wording shown below was added to the first paragraph of page 9:

"Three different batches denoted M-1, M-2 and M-3 were produced using P-A1, P-B1 and P-C1 for M-1, P-A2, P-B2 and P-C2 for M-2 and P-A3, P-B3 and P-C3 for M-3 (where the suffix 1 refers to batch 1, 2 to batch 2 and 3 to batch 3; see Section **Error! Reference source not found.**)."

5. Do you think that if you have used quartz cuvette the result will be similar to that of plastic cuvette?

- There would be some differences especially in the near IR region. To further discuss/clarify, more wording below has been added to the first paragraph of Section 2.4 on page 12:

"Disposable cuvettes (light path length, 10 mm) were used, with base-fluid and cuvette correction being employed. If a quartz rather than plastic cuvette had been employed there would be some differences especially in the IR region. However, for consistency and ease of experimentation plastic cuvettes were used for this study. A full comparison between different optical materials for the cuvettes is beyond the scope of this work but will be assessed in future studies."

6. Th properties presented in table 1 are they for base fluid or nanofluid? And how have they been measured i.e. Cw?

- More information (below) has been added to the end of the second paragraph on page 10 just before Table 1, to make it clear that the heat capacity and mass of the base-fluid were used to approximate the heat capacity and mass of the nanofluid.

"For the dilute nanofluid the values used for heat capacity and mass were taken as approximately the same as the base-fluid (Jin et al., 2016) – hence the values for the base-fluid for these have been shown."

- This has been further specified in the caption for Table 1: "The same values were used for the base-fluid and the nanofluids."

- More wording (below) has also been added to the end of the second paragraph (p.11); Table 1 and all subsequent calculations have been updated to ensure consistency of the value used for C_w, including most of the values in Table 3, where the recalculation has no effect on the grouping.

"The value for C_w was taken as the average value between 20 and 40 °C for water from (Engineering Toolbox, 2004) (See SI Table S4)."

Original Table 3

Nanofluid type	n*	Grouping	Mean PE_{Total} from SSL / %	StDev / %	95% CI for the mean
Water	3	D	20.59	1.17	14.73 – 26.45
M	9	A	84.12	2.30	80.75 – 87.51
P-A	9	B	62.73	4.50	59.35 – 66.11
P-B	9	B	65.33	7.61	61.95 – 68.71
P-C	9	C	47.89	4.70	44.50 – 51.27

Revised Table 3

Nanofluid type	n*	Grouping	Mean PE_{Total} from SSL / %	StDev / %	95% CI for the mean
Water	3	D	20.51	1.17	14.61 – 26.34
M	9	A	83.77	2.29	80.40 – 87.14
P-A	9	B	62.46	4.49	59.09 – 65.83
P-B	9	B	65.05	7.58	61.68 – 68.42
P-C	9	C	47.68	4.68	44.31 – 51.05

- As a results, this has changed the PE_{total} value for M from 84.12% to 83.77%, which has been updated throughout the manuscript where this number is referred to.
- To explain how the other constants in Table 1 were measured, more information has been provide at the end of paragraph 2 on page 11, as follows.

"The surface area exposed was measured with a ruler and the mass of the base fluid calculated from the volume employed (measured with a micro pippette) using a density of 1000 kgm^{-3}."

- The reference to how the Incident radiative intensity I_s was measured, and the reference for the heat capacity were added to Table 1.

7. It can't be qualified the shifting in P-B figure 2 as slight shift! And how do you justify this shift from 667 to 709nm?

- The word "slightly" has been removed. In addition, more discussion has been added to the first paragraph of Section 3.1 on page 13, as follows.

Because of this reduction in stability observed for P-B the amount of P-B in the mixture M was kept to a minimum (see Section **Error! Reference source not found.**). The shift in λ_{max} could be due to morphological changes in the AgNPs with time (a sharpening of the corners of the rounded prisms and or an increase in size could lead to a red shift being observed) and represents additional information, which is obtained from undertaking experimental rather than numerical studies.

8. Are the measured absorption and incident light absorbed are different?

- To clarify and ensure consistency throughout the paper, in the first paragraph of Section 3.3 (p.17), additional wording has been included, i.e. "… power absorbed …".

9. Figure 5, please provide a fundamental explanation on why the absorption amount between 1100-1300nm of the M has been reduced?

- More interpretation/discussion has been added to the first paragraph on page 18, as follows.

The reasons for this are two-fold, firstly the amount of P-A, which is only a weak absorber in this region, in M is only 50% this reduces the power absorbed in this region due to the AgNPs. Secondly, as base-line correction for the base-fluid was used to undertake the UV-Vis-IR measurements any absorption due to the base-fluid water in this region would not be accounted for. As water absorbs more strongly in this region (Mallah et al., 2018), this leads to an under estimation of the power absorbed by the combination of the AgNPs and the base-fluid (i.e. the nanofluid) above 1100 nm.

Reviewer #3: The paper is dedicated to propose a novel mixture of plasmonic silver nanofluids to be employed in a direct absorption solar collector. A broadband absorber was designed through combining three types of nanosilvers with different shapes. Each type covered an specific wavelength range through a plasmonic response. The photo-thermal conversion efficiency and temperature rise of nanofluid indicated significant enhancement compared to water. However, morphology change of such nanoparticles through light exposure declined the nanofluid efficiency. Comments:

1- The optimum calculated combination was reported as 50% P-A, 20% P-B and 30% P-C, how it was estimated?

- Please see response (above) to Reviewer #2 comment 3. More explanation has been added to the text, and an additional Table added to SI.

2- How much were the concentrations of each types of nanofluids? How were these concentrations selected? What were the effect of nanoparticle concentrations?

- More information has been added to Procedure A (P-A) on page 6:

"This synthesis was designed to produce silver nanoparticles (AgNPs) with absorption maxima (λ_{max}) in the 850 - 950 nm range with a final silver concentration of 0.1 mM Ag. This concentration was chosen based on prior knowledge of ease and consistency of synthesis (SI Table S1)."

- More wording added to Procedure B (P-B) on page 6:

"This synthesis was designed to produce AgNPs with absorption maxima in the 650 -700 nm range, with a final silver concentration of 0.3 mM Ag (SI Table S1) again based on prior experimental knowledge to ensure ease and consistency of the reaction."

- More wording added to Procedure C (P-C) on page 7:

"This synthesis was designed to produce disc-shaped small AgNPs with a λ_{max} of 420 -500 nm, with a final silver concentration of 0.457 mM (SI Table S1)."

- More wording has been added to the end of the first paragraph on page 20 to discuss further the effect of nanofluid concentration:

"If the path length or the concentration of M was increased, the performance of this blended nanofluid could be further improved. On the other hand, increasing the concentration may, have a detrimental effect on the colloidal stability. Conversely, reducing the nanofluid concentration would potentially improve colloidal stability, but a greater depth of nanofluid would be needed to give the same performance. This would require further investigation."

- An additional Table has been added to the SI detailing the concentrations and with additional wording added to the SI, as follows.

1 Concentrations of nanofluids

The concentration of silver in the nanofluids employed are given in *Table S1*. Note that this is the concentration of silver in the starting solution and is not necessarily the concentration of nanoparticles. The starting concentrations for P-A, P-B and P-C were selected based on prior knowledge of the synthesis to

ensure ease and consistency of reaction and to give a final H_{peak} of < 1.6 au for the mixture M using a 10 mm path length cuvette without the need to centrifuge to concentrate the nanofluids.

Table S1 Concentration of nanofluids

Nanofluid	Concentration Ag / mM	Concentration Ag / wt% Ag
P-A	0.100	0.00108
P-B	0.300	0.00324
P-C	0.457	0.00493
P-D	0.247	0.00266

- All references to the Tables in the SI have been updated.
- The molarity and wt% Ag values for the calculated mixtures have been added to SI Table S2 (please see above response to Reviewer #2 comment 3).

3- About Figure 7, what was the initial temperature of nanofluid? Please investigate the effect of initial temperature on photo-thermal conversion efficiency of these nanofluids.

- More information about the SSL measurements has been added to the first paragraph on page 10 in the Experimental Methods:

"Care was taken to ensure the starting temperature of the sample was as consistent as possible at 25 °C ± 1.5 °C."

- The measured starting temperature results have been reported in the first paragraph of Section 3.4 (p.20):

"The initial temperature recorded at the start of each experiment was 25.7 °C (StDev 0.6 °C N = 39)."

- More discussion about the possible effect of initial temperature on the PE has been added to the end of the first paragraph on page 21, as follows.

In addition, if care had not been taken to maintain a consistent starting temperature of the nanofluid, there may have been some variation in the length of the linear portion of the graph, requiring that the slope was calculated over a smaller Δt. However, it should not greatly affect the value of PE obtained (especially when the experimental uncertainties of 8.24 – 10.37 % are considered), unless a significantly higher starting temperature at or near the stagnation temperature was used leading to no linear region on the graph. Further investigation of the effect of starting temperature would be needed to confirm this.

4- With respect to the instability of silver nanofluids as shown in figure 10, it is suggested to investigate the temperature effect on morphology change of the nanoparticles.

- The final paragraph of the conclusions has been re-written to prioritise the investigation into the effect of temperature as part of the further work (p.26):

"Further work will firstly focus on the effect of temperature alone on the broadband absorber stability as it is important to determine if the instability is due to the solar radiation or a combination of solar radiation and heat. The focus will then shift to measuring the broadband absorber under flow conditions to get a better understanding of potential performance and stability to mechanical damage."

Reviewer #4: The manuscript presents strategy to increase the efficiency of solar thermal energy capture by the utilisation of three silver nanofluids in a direct absorption solar collector.
Rusults show that photo-conversion efficiency was enhanced by 85% and absorption efficiency by 93%. However silver nanofluids showed instability. The manuscript is well written and complete. Highlights and the Graphical Abstract are also clear.

Comments:
In Experimental methods (2.3 Nanofluids performance under simulated sunlight) the authors should provide experimental tests to calculate the heat capacity of nanofluids even if they are diluted In

- As addressed above to Reviewer 2 comment 6, more discussion and calculation have been presented. Briefly, the heat capacity was approximated to that of the base-fluid (in this case water) as the nanofluids were dilute and this was explained in the text. A more accurate value for C_w (average of value for water at 20 and 40 °C) has now been used and all subsequent calculations updated to reflect this change.

Results and discussion: in TEM images (Fig. 4 and Fig.9) it is not clear if all bars are 100 nm (even bars in the inserts?).

- Clarification has been made for captions of Fig. 4 and Fig. 9; both read: "All scale bars including the ones in the inserts = 100 nm."

In addition, the following changes have been made during the revision.

- A minor error in calculation for Figure 3 has been discovered, thus the Figure 3 has been updated accordingly. All text pertaining to Figure 3 in the manuscript has been checked that is still valid. Figure S4 and Table S12 have also been updated.
- Abbreviations in the caption of Table S4 and in the main body of the table have been checked and corrected for consistency throughout the manuscript. They used to read C_wM_w/IA, and now read C_wM_w/I_sA_s. In Table S4, "I" has been changed to "I_s".
- Reference to SI Tables S9, S10 and S11 have been added to Section 3.1, the first paragraph on page 14.

*Marked Revised Manuscript
Click here to view linked References

Silver nanofluids based broadband solar absorber through tuning nanosilver geometries

Harriet Kimpton[ab], Eugen Stulz[a*], Xunli Zhang[b*]

[a] *School of Chemistry, University of Southampton, University Road, Southampton, SO17 1BJ, UK*

[b] *School of Engineering, University of Southampton, University Road, Southampton, SO17 1BJ, UK*

** Corresponding Authors: X. Zhang (XL.Zhang@soton.ac.uk); E. Stulz (est@soton.ac.uk)*

ABSTRACT

This work explores the strategy for increasing the efficiency of solar thermal energy capture by the utilisation of a blended mixture of plasmonic silver nanofluids in a direct absorption solar collector. For the first time, a broadband absorber based on combining three silver-based nanofluids, each with a tailored plasmonic response covering a different wavelength range, was designed and synthesised. The potential efficiency of this broadband absorber was estimated from the UV-Vis-IR spectra and from direct measurement of the temperature rise obtained in static tests in a solar simulator. The results from the two methods were comparable. The broadband absorber was shown to increase the efficiency of capture compared to the component nanofluids and compared to water. The temperature rise in the solar simulator for the broadband mixture was more than four times that of water and the photo-thermal conversion efficiency was approximately 85%, demonstrating the promise of this mixture for enhancing solar energy capture. However, this work also illustrates the potential issues with utilising silver for solar applications, namely the change in morphology and UV-Vis-IR spectra with light exposure. A suitable stabilisation or coating strategy would hence be required to use this developed broadband absorber in solar energy applications.

Keywords: Nanofluids; Plasmonic; Broadband solar absorber; Stability; Silver nanoprisms; Silver nanodiscs

Author declaration: This publication has no known conflicts of interest. Its outcome was not influenced significantly by any financial support.

Abbreviations:

AE	Absorption efficiency / %
A_s	Surface area
AgNPs	Silver nanoparticles
ANOVA	Analysis of variance
A_λ	Absorption at wavelength λ
CI	Confidence interval
C_w	Base-fluid heat capacity / Jkg^{-1} K^{-1}
DASC	Direct absorption solar collector
H_{Peak}	Height of maximum absorption peak / au
IR	Infra-red
I_s	Incident radiative intensity / Wm^{-2}
M	Mixture
M_w	Base-fluid mass / kg
$P_{Ab(\lambda)}$	Power absorbed at wavelength λ / Wm^{-2}
PE_{Total}	Total photo-thermal conversion efficiency / %
$P_{i(\lambda)}$	Incident power intensity at λ / Wm^{-2}
$P_{T(\lambda)}$	Power transmitted at wavelength λ / Wm^{-2}
PVP	Polyvinylpyrrolidone
SI	Supplementary information
SSL	Simulated sunlight
StDev	Standard deviation
TEM	Transition electron microscopy
TSCD	Tri-sodium citrate dehydrate

UV	Ultraviolet
wks	Week
wt %	weight / %
Δt	Change in time / s
ΔT	Temperature change / °C
λ_{max}	Wavelength of maximum absorption peak / nm

1 INTRODUCTION

Direct absorption solar collectors (DASCs), proposed initially in the 1970's (Minardi and Chuang, 1975), are designed to directly absorb solar thermal energy into a volume of liquid which is also used as the working fluid for subsequent heat transfer. Compared to the traditional selective absorbing surface collectors (Gupta et al., 2015) DASCs have a number of advantages, namely, simpler manufacturing, improved heat transfer and reduced heat loss due to an even temperature distribution in the fluid (Iyahraja and Rajadurai, 2015; Lee et al., 2016; Luo et al., 2014; Otanicar and Golden, 2009; Otanicar et al., 2010; Tyagi et al., 2009; Xu et al., 2015). These factors have led to an overall increase in collector efficiency of about 10% (Nasrin et al., 2015; Turkyilmazoglu, 2016).

However, without additions the working fluids employed in most DASCs only absorb a low percentage of the solar radiation in the range of 2% to 14% over the wavelength range 200 - 1500 nm (Otanicar et al., 2009). This can be overcome by the addition of Indian ink or micro particulate carbon (Gorji and Ranjbar, 2016) but the addition of large particles can cause issues with sedimentation, erosion and pump blockages (Kazemi-Beydokhti et al., 2014; Khullar et al., 2014). Hence, in recent years there has been considerable interest in the use of nanoparticles to engineer colloidal nanofluids with superior absorption characteristics, small particle sizes and low concentrations. In this aspect, metallic nanoparticles that exhibit surface plasmonic resonance at certain wavelengths can improve absorption characteristics while maintaining a very low

nanoparticle concentration, and improving colloidal stability (Ahmad et al., 2017; Du and Tang, 2016).

The plasmonic response of metallic nanoparticles only occurs at certain wavelengths, depending on the shape and size of the particles used, thus leading to narrow spectra absorption. To overcome this limitation a blend of different plasmonic nanoparticles can be used as a broadband absorber with enhanced absorption at low nanoparticle concentration. For example, blended gold nanorods with different aspect ratios (Jeon et al., 2014; Jeon et al., 2016) and mixtures of gold nanorods with ellipsoids and nanosheets (Du and Tang, 2016) have been studied as plasmonic broadband absorbers for DASC and other solar applications. A blended nanofluid has been concepted as the ideal broadband solar absorber for DASC applications (Goel et al., 2020; Sharaf et al., 2019), and two silver broadband mixtures comprising five different silver nanoparticle geometries have been investigated numerically (Mallah et al., 2018). Their two blended nanofluids gave absorption efficiencies of 98 % and 95 % respectively over the range of 300-2500 nm for a nanofluid depth of 10 cm. This work complements this numerical work, using a simpler three component mixture, but provides additional information on issues that occur when mixtures of different nanoparticle geometries are combined together experimentally. The concept of a broadband absorber based on silver is not novel, but to the authors' best knowledge the experimental production and subsequent testing of such a blended broadband absorber mixture has not been reported.

The surface plasmonic response of silver nanoparticles, similar to other metallic particles is highly dependent on the size and shape of the nanoparticles in the nanofluid (Aherne et al., 2008; Haber and Sokolov, 2017; Ledwith et al., 2007). Most experimental studies for DASC applications have focused on nanospheres (Abdelrazik et al., 2019) with a strong absorption around 400 nm and have shown efficiency improvements of between 5 % and 144% (Bandarra Filho et al., 2014; Chen et al., 2016; Otanicar et al., 2010), compared to water. Some work has also been carried out on anisotropic silver nanodiscs with a plasmonic response at about 650 nm for volumetric absorption (Crisostomo et al., 2017; Hjerrild et al., 2018; Taylor et al., 2018). Interestingly, Walshe et al "accidentally" produced a silver nanofluid with two different absorption peaks at approximately 430 and 600 nm which gave a good photo-thermal conversion efficiency (PE) of 70% - 90% depending on nanoparticle concentration (Walshe et al., 2019).

In our series of research on silver nanoparticles, we have focused on producing consistently silver nanoprisms with a strong absorption in the near infra-red (Carboni et al., 2013; Carboni et al., 2016; Mabey et al., 2019; Zmijan et al., 2014). This development has provided us with necessary fundamental understanding and practical tools to design and produce a blended silver broadband absorber consisting of a number of component nanofluids containing different sizes and shapes of silver nanoparticles for desired plasmonic responses. There are a range of methods for controlling the morphology and hence position of the plasmonic absorption for silver nanoparticles, such as photo-mediated methods (Bastys et al., 2006; Tang et al., 2009; Tang et al., 2013) and various chemical methods (both direct and utilising a silver seed solution) (Aherne et al., 2008; Haber and Sokolov, 2017; Ledwith et al., 2007). In the work with a modified direct chemical method (Zhang et al., 2011), the reduction of silver ions were carried out with sodium borohydride in the presence of hydrogen peroxide to give nanoprisms The amount and timing of the addition of the reagents was adjusted to vary the size and shape of the particles produced.

The aim of the present study was to demonstrate the proof-of-principle of utilising a broadband, blended plasmonic absorber for DASC applications based on silver nanofluid. Three types of silver nanofluids with different size and shape of nanoparticles were synthesised with plasmonic responses in the range of 880 - 980 nm, 650 - 750 nm and 450 - 520 nm, respectively. These were blended to give a mixture for broadband solar absorption. The solar performance of individual component nanofluids and their broadband mixture were then assessed by using ultraviolet-visible-infrared (UV-Vis-IR) spectroscopy and a solar simulator, hence providing quantitative evaluation towards solar energy capture applications. This study was designed, for the first time, to create a broadband absorber utilising silver nanoparticles with a tailored absorption profile to match the solar spectrum in the Vis-IR range by physically blending three separate nanofluids. It was also the first time that the performance of this novel nanofluid was investigated in static tests utilising a solar simulator, and further compared with theoretical spectroscopy analysis and calculations.

2 EXPERIMENTAL METHODS

2.1 Chemicals

All chemicals were sourced from Sigma Aldrich. They were used as purchased and consisted of: Sodium borohydride ($NaBH_4$, 99%), hydrogen peroxide (H_2O_2 30 weight percentage (wt.%)), silver nitrate ($AgNO_3$ 99%), Polyvinylpirrolidone (PVP, average molecular weight ≈ 29,000 g mol^{-1}), and tri-sodium citrate dihydrate (TSCD). Milli-Q water was used throughout.

2.2 Synthesis

Procedure A (P-A): This synthesis was designed to produce silver nanoparticles (AgNPs) with absorption maxima (λ_{max}) in the 850 - 950 nm range with a final silver concentration of 0.1 mM Ag. This concentration was chosen based on prior knowledge of ease and consistency of synthesis (SI Table S1). The synthesis was based on that employed by Zhang *et al* (Zhang et al., 2011) with some modifications, where AgNPs were stabilised with both PVP and TSCD (Kimpton et al., 2020). Briefly, 24 mL aqueous solution comprising of hydrogen peroxide (H_2O_2, 30 wt.%, 0.125 mL), silver nitrate ($AgNO_3$, 0.05 M, 0.05 mL), PVP (0.70 mM, 0.375 mL) and TSCD (0.10 M, 0.375 mL) was vigorously agitated at room temperature using a magnetic stirrer for 7 minutes. That was followed by rapidly injecting a newly prepared sodium borohydride solution ($NaBH_4$, 25.00 mM, 1.00 mL). It took another 30 minutes of stirring for the reaction to then proceed via a noticeable colour change with gas evolution, through light yellow to orange, brown-orange, and blue-green and finally to blue over a further period of 5 - 10 minutes.

Three batches of PVP and TSCD stabilised AgNPs (25 mL each) were produced (labelled P-A1, P-A2 and P-A3, respectively). A Perkin Elmer Lambda 750S UV-Vis-IR spectrophotometer was used to acquire the spectra of the batches. A 10 mm light path length cuvette was employed.

Procedure B (P-B): This synthesis was designed to produce AgNPs with absorption maxima in the 650 -700 nm range, with a final silver concentration of 0.3 mM Ag (SI Table S1) again based on prior experimental knowledge to ensure ease and consistency of the reaction. The synthesis employed for Procedure A was adapted by reducing the ratio of sodium borohydride to produce more rounded triangular AgNPs while also increasing the starting concentration of silver, PVP and

TSCD in solution. Briefly, 23.5 mL of solution containing TSCD (0.10 M, 1.125 mL), silver nitrate ($AgNO_3$, 0.05 M, 0.15 mL), PVP (0.70 mM, 1.125 mL) and hydrogen peroxide (H_2O_2, 30 wt.%, 0.375 mL) was stirred vigorously at room temperature. After 7 minutes a freshly prepared solution of sodium borohydride ($NaBH_4$, 25.00 mM, 1.5 mL) was rapidly injected. After about 15 minutes, the solution colour changed rapidly through yellow to orange-brown, then through to green-blue after a further 5 - 10 minutes.

With three 25 mL batches (denoted P-B1, P-B2, and P-B3, respectively) of TSCD and PVP stabilised AgNPs produced, UV-Vis spectra (using a Perkin Elmer Lambda 750S UV-Vis-IR spectrophotometer) of each batch were recorded. The samples were diluted to 1 mL in 3 mL with Milli-Q water prior to measuring the spectra to prevent saturation of the detector and a 10 mm cuvette was employed.

Procedure C (P-C): This synthesis was designed to produce disc-shaped small AgNPs with a λ_{max} of 420 -500 nm, with a final silver concentration of 0.457 mM (SI Table S1). Firstly, AgNPs were synthesised using Procedure B but with half the H_2O_2 amount. These were then used as a starting point to produce smaller AgNP discs by the addition of more silver and reducing agent. Briefly, 23.5 mL of solution containing TSCD (0.10 M, 1.125 mL), silver nitrate ($AgNO_3$, 0.05 M, 0.15 mL), PVP (0.70 mM, 1.125 mL) and hydrogen peroxide (H_2O_2, 30 wt.%, 0.188 mL) was stirred vigorously at room temperature. After 7 minutes a freshly prepared solution of sodium borohydride ($NaBH_4$, 25.00 mM, 1.5 mL) was rapidly injected. After about 15 minutes, the solution colour changed rapidly through yellow to orange-brown, then through to green-blue after a further 5-10 minutes. More silver nitrate ($AgNO_3$, 0.05 M, 0.083 mL) was then added, with vigorous stirring followed by the rapid injection of more sodium borohydride ($NaBH_4$, 25.00 mM, 0.42 mL). Again, with three batches (denoted P-C1, P-C2 and P-C3, respectively) UV-Vis-IR spectroscopy was undertaken. The samples (0.6 mL) were diluted with Milli-Q water to give a total volume of 3.0 mL to prevent saturation of the detector with a 10 mm cuvette employed for the UV-Vis-IR spectroscopy measurement.

Mixture (denoted M): The UV-Vis-IR spectra obtained from P-A, P-B and P-C were used to calculate the best combination of all three components to give as high a percentage coverage of the solar spectra as possible. The solar reference spectra utilised was the direct + circumsolar

spectrum from ASTM G173 (ASTM, 2012). This was used as a reference to calculate how much of the solar spectrum was covered by the mixture.

In physics, from Beer's law, absorption of light is a measure of how matter takes up a photon's energy at a given wavelength λ, that is expressed by the following formula (Khullar et al., 2014; Sheffield Hallam University, 2019):

$$A_\lambda = log_{10} \frac{P_{i(\lambda)}}{P_{T(\lambda)}}$$

Equation 1

where A_λ is the absorption at wavelength λ (au); $P_{i(\lambda)}$ is the incident power intensity at λ in Wm^{-2}; and $P_{T(\lambda)}$ is the power transmitted at wavelength λ (Wm^{-2}). Hence Power absorbed $P_{Ab(\lambda)}$ in Wm^{-2} at a given wavelength is:

$$P_{Ab(\lambda)} = P_{i(\lambda)} - \frac{P_{i(\lambda)}}{10^{A_\lambda}}$$

Equation 2

The absorption efficiency (AE) over the wavelength range (300-1350 nm) is then obtained by dividing the sum of the power absorbed by the sample, $\sum_{\lambda=300}^{\lambda=1350} P_{Ab(\lambda)}$, by the total incident power over the wavelength measured, $\sum_{\lambda=300}^{\lambda=1350} P_{i(\lambda)}$, according to the formula (Du and Tang, 2016; Duffie and Beckman, 2013; Modest, 2003):

$$AE_{(300-1350nm)} = \frac{\sum_{\lambda=300}^{\lambda=1350} P_{Ab(\lambda)}}{\sum_{\lambda=300}^{\lambda=1350} P_{i(\lambda)}} \times 100$$

Equation 3

where $\sum_{\lambda=300}^{\lambda=1350} P_{i(\lambda)}$ = 793.1 Wm^{-2} (taken from the Reference Solar Spectral Irradiance G173 spectra (ASTM, 2012)). It should be noted that the apparatus employed only allowed the measurement of the broadband absorber over the 300 – 1350 nm range which accounts for 88.1% of the power of the total solar spectrum from 280 to 4000 nm. Hence $P_{i(280\text{-}4000nm)}$ = 900.2 Wm^{-2}.

The $AE_{(300\text{-}1350nm)}$ obtained for various mixtures were calculated using the average UV-Vis-IR spectra for the various components and Equations 1-3 and are given in SI Table S2. The selected calculated combination whilst minimising the amount of P-B (the least stable nanofluid in the mixture) was 50% P-A, 20% P-B and 30% P-C, that equates to 0.247 mM final silver concentration in the mixture. This gave a value of $AE_{(300\text{-}1350nm)}$ of 82.52 % which was slightly lower than the optimum mixture without minimizing P-B of 83.14 % (Table S2). Three different batches denoted M-1, M-2 and M-3 were produced using P-A1, P-B1 and P-C1 for M-1, P-A2, P-B2 and P-C2 for M-2 and P-A3, P-B3 and P-C3 for M-3 (where the suffix 1 refers to batch 1, 2 to batch 2 and 3 to batch 3: see Section 2.2). The UV-Vis-IR spectra for the three M batches were then recorded along with transition electron microscopy (TEM) imaging.

2.3 Nanofluids performance under simulated sunlight (SSL)

The set-up of the sunlight simulating system is schematically shown in Figure 1Figure 1. A stabilised power supply (160H x 210L x 200W mm) connected to a xenon light source (output 50 W, collimated spot 30-63 mm diameter, 300-500 nm range), both supplied by Perfect Light Ltd in China, was used to simulate sunlight (model CHF-XM-500W with a PLS SXE300 lamp). Cooling was provided by both a metal fan and radially. The lamp output variation was ± 6 %. A constant setting was used giving a light intensity of 1191 ± 40 Wm^{-2} (measured using a ReRA system calibrated PV cell see SI Table S3).

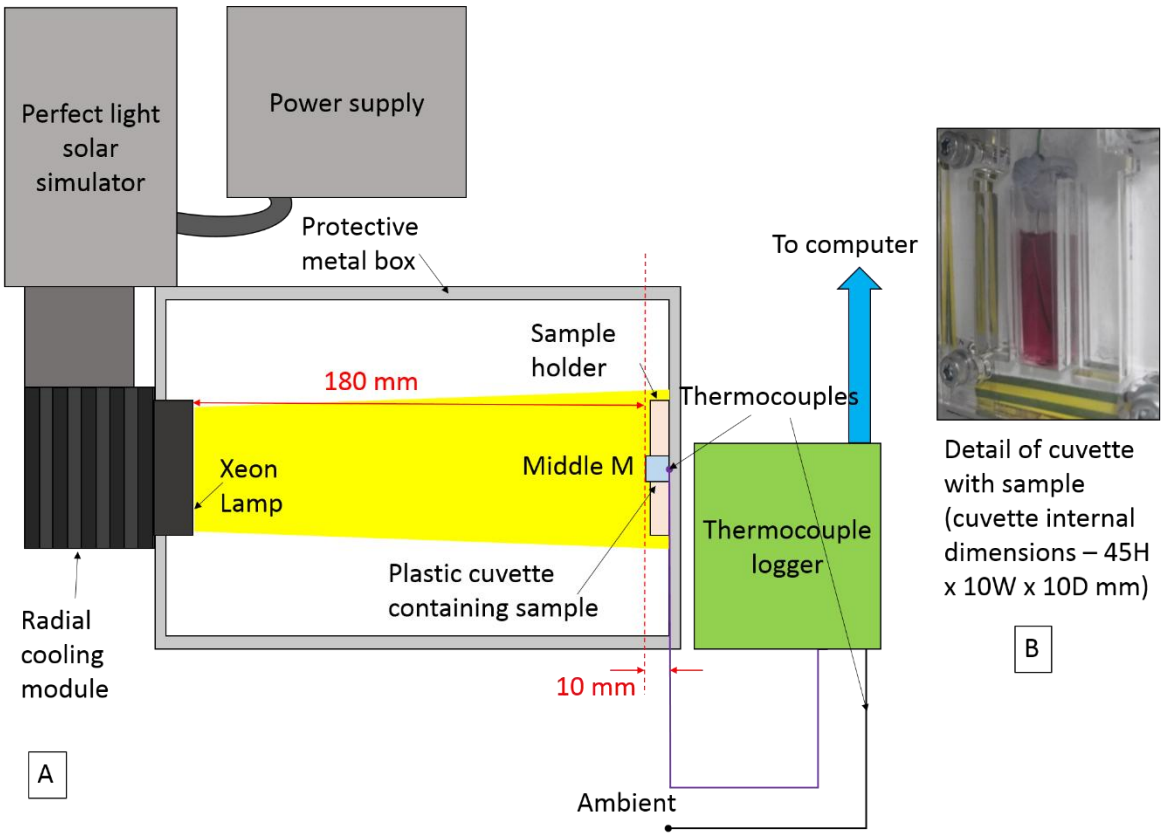

Figure 1 A – Schematic of solar simulator set-up and B – Photograph of sample in cuvette holder with thermocouple

To cover the lamp and provide consistent sample placement (180 mm from lamp to front face of sample) a modified steel metal box was used (300L x 250H x 150D mm, Schneider Electric, Farnell). A sample holder was designed and laser cut from a Perspex sheet. It was bolted to the steel box using 10 mm bolts (not shown) so that the centre of the sample holder was in the centre of the light beam. The temperature of the sample was monitored in real-time using an RS PRO type K thermocouple (diameter 0.6 mm, temperature ranging from –50 to +250 °C) with a welded grounded junction conforming to IEC 60584 standard. Care was taken to ensure the starting temperature of the sample was as consistent as possible at 25 °C ± 1.5 °C. The thermocouple was placed 10 mm from the front face of the sample (see Figure 1A and photograph Figure 1B). The thermocouple was connected to a PC via a National Instruments NI9211 thermocouple data logger with LabVIEW software.

With three batches of P-A, P-B and P-C, and one mixture M prepared the performance under SSL was characterised. Samples P-A and M were measured as prepared, while 1 mL P-B was diluted to

3 mL total volume with water, and 0.6 mL P-C was diluted to 3 mL total volume. The resulting nanofluids were examined before and after SSL exposure using UV-Vis-IR spectroscopy and TEM.

For measurements, a solvent resistant disposable cuvette (Figure 1B) containing 3 mL of sample and the thermocouple was sealed using blue tack and parafilm to prevent evaporation and placed in the sample holder. Samples were exposed to SSL for a period of 10 minutes and then cooled. The measurement was repeated two more times. The UV-Vis-IR spectrum of the sample was then recorded as detailed in Section 2.4. The change in temperature (ΔT) was obtained, as well as the slope of the graph ΔT/Δt in the linear range of the time period (t = 91 - 211 seconds). For a diluted nanofluid, the heat capacity and the mass of nanofluid can be approximated by the heat capacity and mass of the base-fluid. The solar absorption performance in terms of photo-thermal conversion efficiency (PE_{Total}) is determined by Equation 4 (Jin et al., 2016):

$$PE_{Total} = \frac{M_w C_w \Delta T}{A_s I_s \Delta t}$$

Equation 4

where PE_{Total} (%) is the increase in internal energy to total incident solar radiation ratio. The mass of base-fluid is M_w (kg); the base-fluid heat capacity is C_w ($Jkg^{-1}\ K^{-1}$); the temperature change is ΔT (K); the exposed surface area is A_s (m^2), the incident radiative intensity is I_s (Wm^{-2}); and the change in time is Δt (s). The values employed for A_s, M_w, C_w and I_s are shown in Table 1. For the dilute nanofluid the values used for heat capacity and mass were taken as approximately the same as the base-fluid (Jin et al., 2016) – hence the values for the base-fluid for these have been shown. The value for C_w was taken as the average value between 20 and 40 °C for water from (Engineering Toolbox, 2004) (See SI Table S4). The surface area exposed was measured with a ruler and the mass of the base fluid calculated from the volume employed (measured with a micro pippette) using a density of 1000 kgm^{-3}.

Table 1 Values used for the constants in Equation 4. The same values were used for the base-fluid and the nanofluids.

Parameter	Symbol	Unit	Value used
Incident radiative intensity (SI Table S3)	I_s	Wm^{-2}	1191
Surface area exposed	A_s	m^2	0.0003

Heat capacity (Engineering Toolbox, 2004)	C_w	$Jkg^{-1}K^{-1}$	4182
Mass of base fluid	M_w	kg	0.003

The spectra obtained from the Xenon lamp was measured using an Avantes AvaSpec-ULS2048 portable spectroscope (wavelength range: 330 - 1100 nm) and AvaSoft 8 software. The AE for the solar simulator lamp ($AE_{Lamp\ (330\text{-}1100\ nm)}$) was calculated utilising this spectra and the UV-Vis-IR spectra obtained for the mixture and components according to Equation 5 where $\sum_{\lambda=330}^{\lambda=1100} P_{i\ lamp(\lambda)}$ is the incident power intensity of the lamp over the wavelength range 330 – 1100 nm. As the spectroscope does not give a power intensity, the spectra obtained for the lamp was normalised, and then the area under the spectral curve was used to approximate $\sum_{\lambda=330}^{\lambda=1100} P_{i\ lamp(\lambda)}$.

$$AE_{Lamp\ (330-1100\ nm)} = \frac{\sum_{\lambda=330}^{\lambda=1100} P_{Ab(\lambda)}}{\sum_{\lambda=330}^{\lambda=1100} P_{i\ lamp(\lambda)}} \times 100$$

Equation 5

The calculated $AE_{Lamp\ (330\text{-}1100\ nm)}$ was then compared to the value of PE_{Total} obtained from Equation 4.

2.4 Characterisation of nanofluids and nanoparticles

UV-Vis-IR spectroscopy analysis was performed with a spectrophotometer (Perkin Elmer Lambda 750S) over a wavelength range of 300 - 1300 nm at a scan rate of 204.74 nm min^{-1}, and a scan step of 1 nm s^{-1}. Disposable cuvettes (light path length, 10 mm) were used, with base-fluid and cuvette correction being employed. If a quartz rather than plastic cuvette had been employed there would be some differences especially in the IR region. However, for consistency and ease of experimentation plastic cuvettes were used for this study. A full comparison between different optical materials for the cuvettes is beyond the scope of this work but will be assessed in future studies.

A Hitachi HT7700 100 kV was used for Transmission electron microscope (TEM) analysis. Samples were prepared on Formvar and carbon coated 200 mesh Cu/Pd grids by drop-casting the colloid

solution and allowing the base-fluid to evaporate. Digimizer software was used to further analyse the samples using the TEM image scale bar to calibrate the line length. Manual size measurement of individual nanoparticles was employed, dividing the particles into different shape categories. For triangular particles, the length of the longest side of the triangle was measured and for discs or spheres, the diameter. Using more than one image of each sample provided a statistically adequate number of measurements.

2.5 Uncertainty analysis

The method employed by (Bell, 2001) and used previously (Kimpton et al., 2020)was used to determine the measurement uncertainty. The calibration / resolution equipment uncertainties (type B) were estimated for the three measurement types (SSL, TEM and UV-Vis-IR). These were added to the sample variation (type A) uncertainties providing a combined relative uncertainty. A final expanded uncertainty was then obtained by using a coverage factor of 2 (about 95% confidence).

The constant M_wC_w/A_sI_s (Equation 4) uncertainties for the SSL tests (type B) resulted in an expanded uncertainty of 8.18 % (SI Table S4). When combined with the sample variation (SI Table S5) the uncertainty range was between 8.24 and 10.37 %. Type B uncertainties from the UV-Vis-IR measurements and subsequent AE calculations were much lower being < 1% (See SI Table S6), giving a combined total when the type A sample variations were added (SI Table S7) of between 1.18 and 6.69%. The type B uncertainties arising from the TEM measurements were <3%. Even with the use of multiple images to increase the number of measurements the particle size variation gave rise to larger type A variation and hence expanded uncertainty (shown for P-A triangles before SSL in SI Table S8) – giving expanded uncertainties of between 6.03 and 9.10% for the TEM measurements. This value does not account for any errors associated with choosing the particle shape manually from the TEM image.

3 RESULTS AND DISCUSSION

3.1 UV-Vis-IR characterisation

The UV-Vis-IR characterisation of the three nanofluids prior to mixing are shown in Figure 2. The mean values of the three repeats are shown both initially and after storage in the dark at 4°C for 4 weeks (individual results are reported in SI, Figures S1, S2 and S3, Tables S9, S10 and S11). As can be seen, three nanofluids exhibited distinguishing spectra with clearly three different positions of corresponding maximum absorption peak (λ_{max}). For nanofluid P-A, λ_{max} was 929 ± 31.8 nm initially. After 4 weeks of storage the mean value remained approximately the same. The peak height (H_{peak}) was 1.577 ± 0.03 au initially, with a slight drop to 1.538 ± 0.02 au after 4 weeks. For nanofluid P-B, λ_{max} was initially 667 ± 7.9 nm with an H_{peak} of 1.342 ± 0.03 au. After 4 weeks of storage in the dark, λ_{max} red shifted to a value of 709 ± 6.1 nm while H_{peak} stayed approximately the same. Finally, for nanofluid P-C, λ_{max} was 468 ± 24.8 nm initially, and 472 ± 23.4 nm after 4 weeks whereas H_{peak} was 0.708 ± 0.06 au initially, and 0.709 ± 0.03 au without noticeable change after storage. The only significant change (see SI for significance testing) was the noticeable red shift in λ_{max} for P-B. Because of this reduction in stability observed for P-B the amount of P-B in the mixture M was kept to a minimum (see Section 2.2). The shift in λ_{max} could be due to morphological changes in the AgNPs with time (a sharpening of the corners of the rounded prisms and or an increase in size could lead to a red shift being observed) and represents additional information, which is obtained from undertaking experimental rather than numerical studies. Nevertheless, the measurements before and after 4 weeks storage showed all three colloidal nanofluids to be relatively stable, with a higher level of stability than that previously observed for colloidal silver (Haber and Sokolov, 2017).

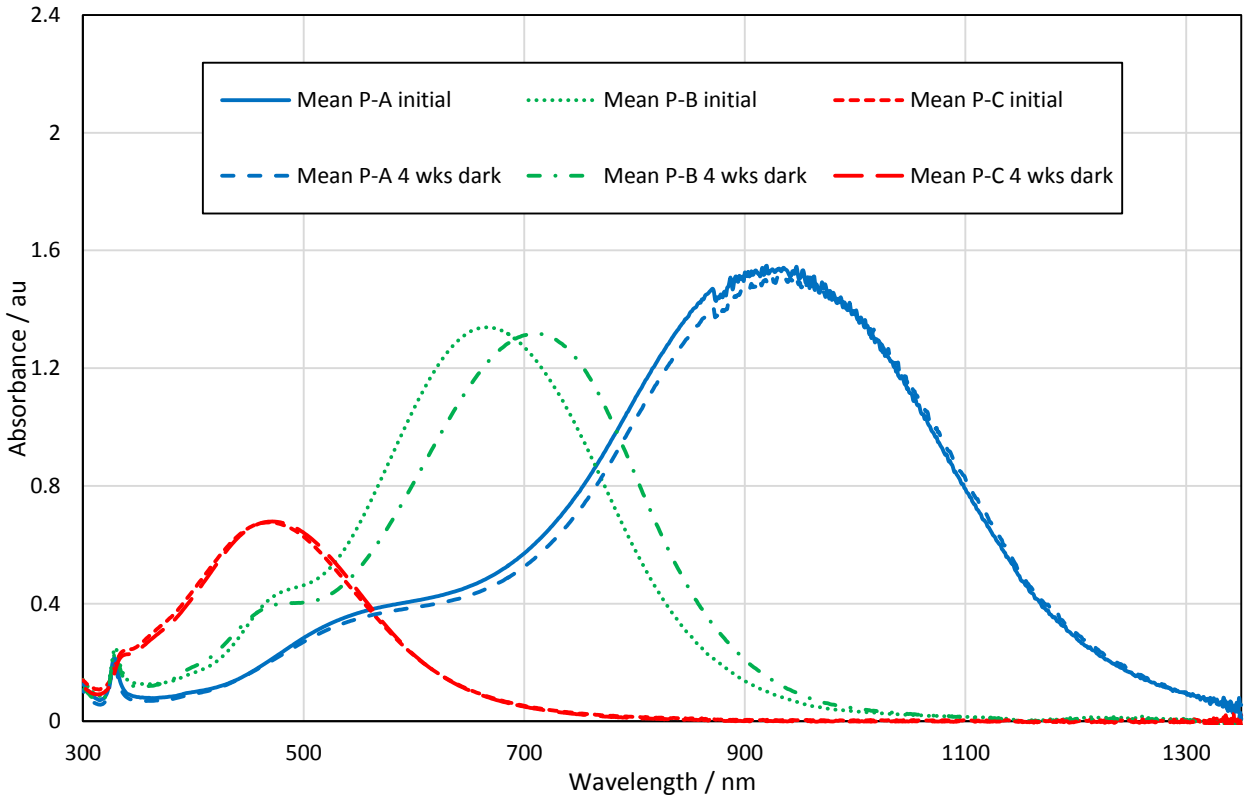

Figure 2 UV-Vis-IR spectra for P-A, P-B and P-C initially, and after 4 weeks storage in the dark at 4°C (4 wks dark). Mean values shown. Note that P-B was diluted 1 mL in 3 mL, and P-C was diluted 0.6 mL in 3 mL. All measurements undertaken with a 10 mm path length cuvette.

Figure 3 shows the results of calculating the absorbance for the mixture based on the spectra obtained for the P-A, P-B and P-C components along with the actual spectra obtained when the mixture was measured (both initially and after storage in the dark at 4°C). Again, the mean values are shown (for the individual values please see SI Figures S4 and S5 and Table S12). For the actual mixture there was a red shift of about 100 nm in the secondary λ_{max} corresponding to the P-B component compared to the calculated value. The primary λ_{max} due to component P-C in contrast was similar for both the calculated and measured spectra. The cause of the red shift in the secondary λ_{max} is unknown but may be related to the smaller but similar red shift observed on storage for P-B and is additional information which is obtained by carrying out experimental studies. This shift was consistent across the three M samples (see Figures S4 and S5). The mixture was, however, stable with storage for 4 weeks in the dark, with no shift in the primary or secondary λ_{max} being observed (see Figure S5 and Table S13).

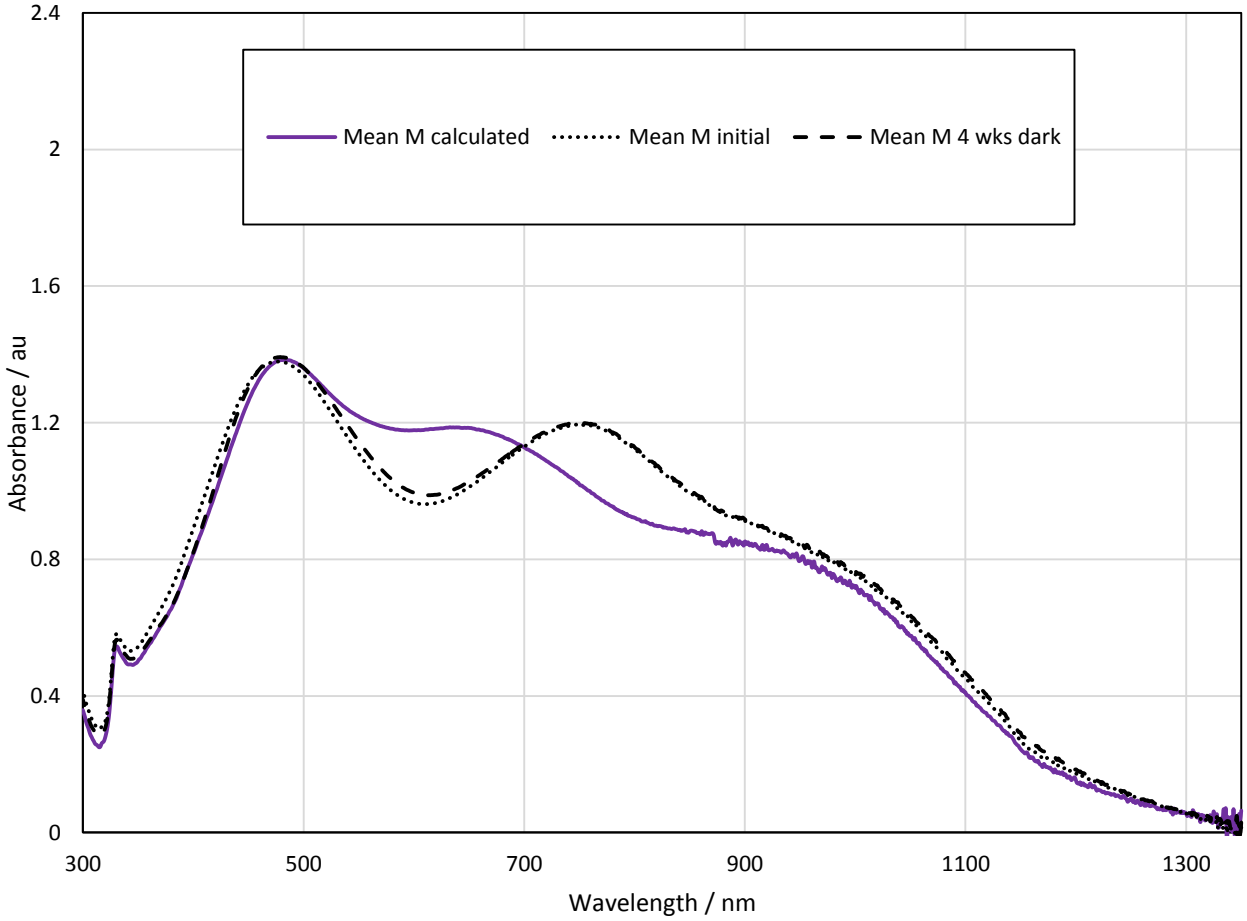

Figure 3 UV-Vis-IR spectra for the mixture M, calculated from the component spectra and as measured initially and after 4 weeks storage in the dark at 4°C. Mean values shown. All measurements undertaken with a 10 mm path length cuvette.

3.2 TEM analysis of as produced nanofluids

TEM analysis of samples P-A, P-B, P-C and the mixture M (Figure 4 and SI Table S14) showed that P-A consisted primarily of triangles with sharp corners with a mean size of 52.2 ± 17.6 nm and a thickness of 5.9 ± 2.6 nm. P-B consisted mainly of smaller triangles (mean size 27.5 ± 7.6 nm) and rounded cornered triangles (mean size 23.7 ± 6.7 nm) which were slightly thinner (mean thickness 4.7 ± 1.3 nm). P-C consisted mainly of small (< 10 nm) particles and slightly larger disc-like particles (diameter 15.9 ± 4.2 nm, thickness 5.0 ± 1.1 nm). As expected the mixture M (Figure 4 D) contained all types of particles, with larger sharp cornered triangles, smaller rounded corner triangles, disc-like particles and small (< 10 nm) particles being present.

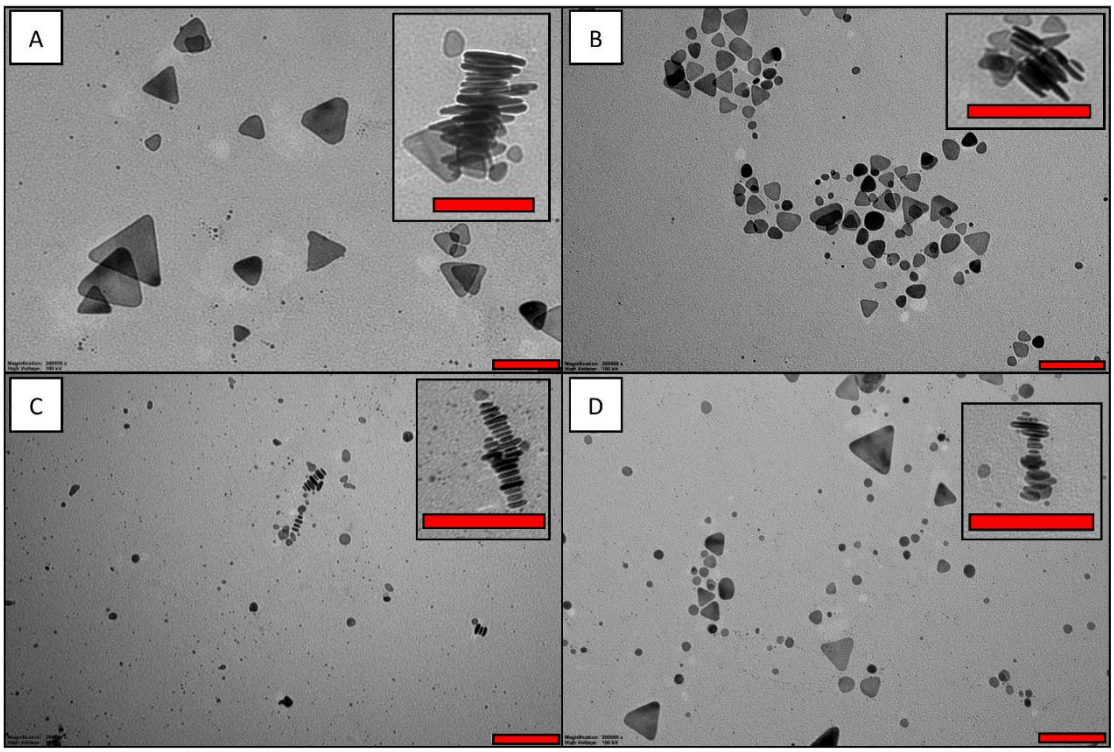

Figure 4 TEM images of A) P-A, B) P-B, C) P-C and D) M before solar simulator testing. The magnified inserts show the edges and thicknesses of the nanoparticles. All scale bars including the ones in the inserts = 100 nm

3.3 Calculating the performance of nanofluids from UV-Vis-IR spectra based absorption

In this work the measured absorption was used directly to calculate the power absorbed rather than the extinction coefficient used by others (Jeon et al., 2014). This approach, on one hand, overcame the difficulty of estimating the extinction coefficient for non-spherical metallic particles (while only spherical and nanorods have been estimated previously) (Gorji and Ranjbar, 2017; Jeon et al., 2014). It was valid as absorption was representative of extinction coefficient for nanofluids of low particle loading without aggregation (i.e. with insignificant scattering effect)(Gorji and Ranjbar, 2015, 2017). On the other hand, it was difficult to compare the results obtained in this work with those reported through extinction coefficient estimation.

According to Equation 2, from the absorption spectra, the power absorbed at different wavelengths relative to the incident solar power intensity can be calculated. The results for three component nanofluids, i.e. P-A, P-B and P-C, and the mixture M, are shown graphically in Figure 5. The calculated value for M and the power intensity not absorbed by the mixture are also shown. Here it can be seen that M absorbs a larger proportion of the power than each of the three

components over a broader wavelength range up to about 1100 nm. In the 1100 – 1350 nm range the performance of the mixture reduced, with only a small proportion of the incident solar power being absorbed. The reasons for this are two-fold, firstly the amount of P-A, which is only a weak absorber in this region, in M is only 50% this reduces the power absorbed in this region due to the AgNPs. Secondly, as base-line correction for the base-fluid was used to undertake the UV-Vis-IR measurements any absorption due to the base-fluid water in this region would not be accounted for. As water absorbs more strongly in this region (Mallah et al., 2018), this leads to an under estimation of the power absorbed by the combination of the AgNPs and the base-fluid (i.e. the nanofluid) above 1100 nm.

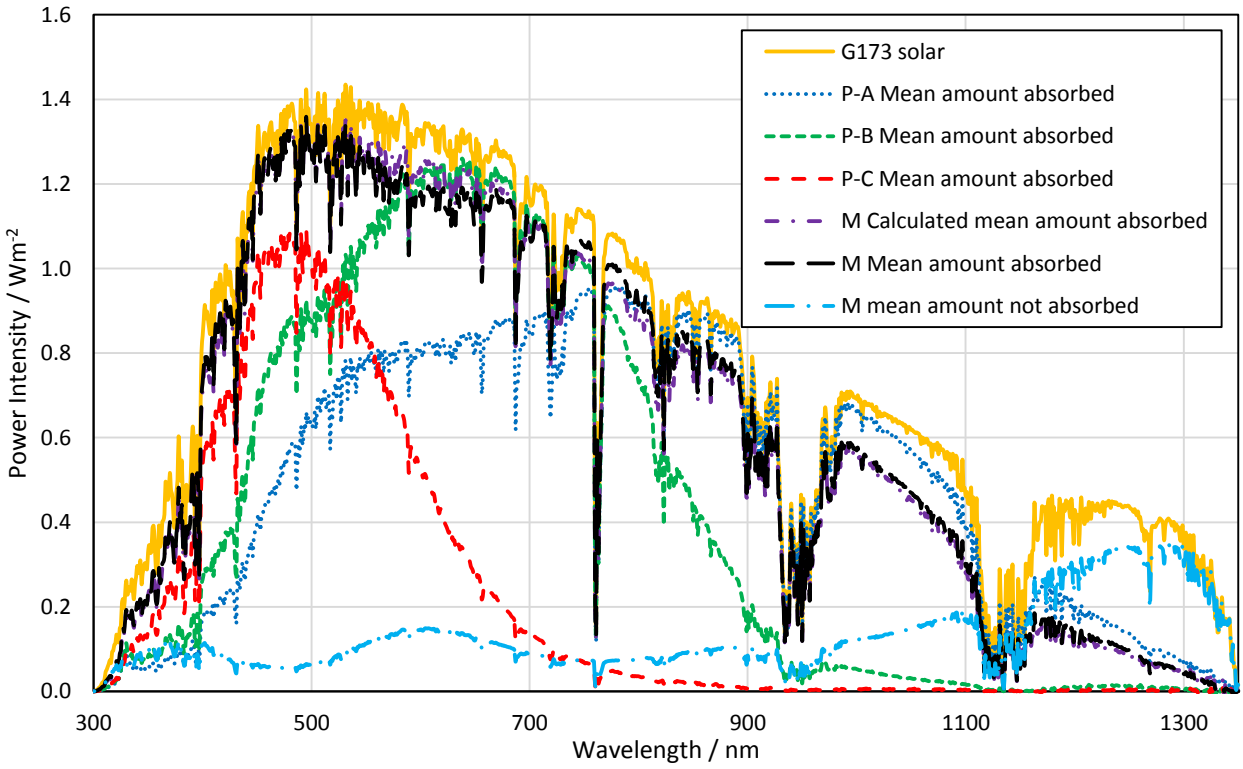

Figure 5 Amount of the G173 solar reference spectral power absorbed at different wavelengths by P-A, P-B, P-C and M. Mean results shown (Complete results given in SI Figures S6 – S10). The amount of the solar spectrum not absorbed by the mixture M is also shown. Calculation uses the same dilution for P-B and P-C as used for the UV-Vis-IR measurements

A comparison between the spectral response of the lamp used for the SSL testing and the G173 Solar spectrum is given in Figure 6. Here it can be seen that there are some differences between the two spectra especially in the 800 – 1100 nm range. Because of these differences $AE_{Lamp\ (330\text{-}1100\ nm)}$ was calculated (see Equation 5) from the UV-Vis-IR spectra to allow comparison with the

results obtained for PE_{Total} obtained from direct measurement of the temperature rise in the solar simulator.

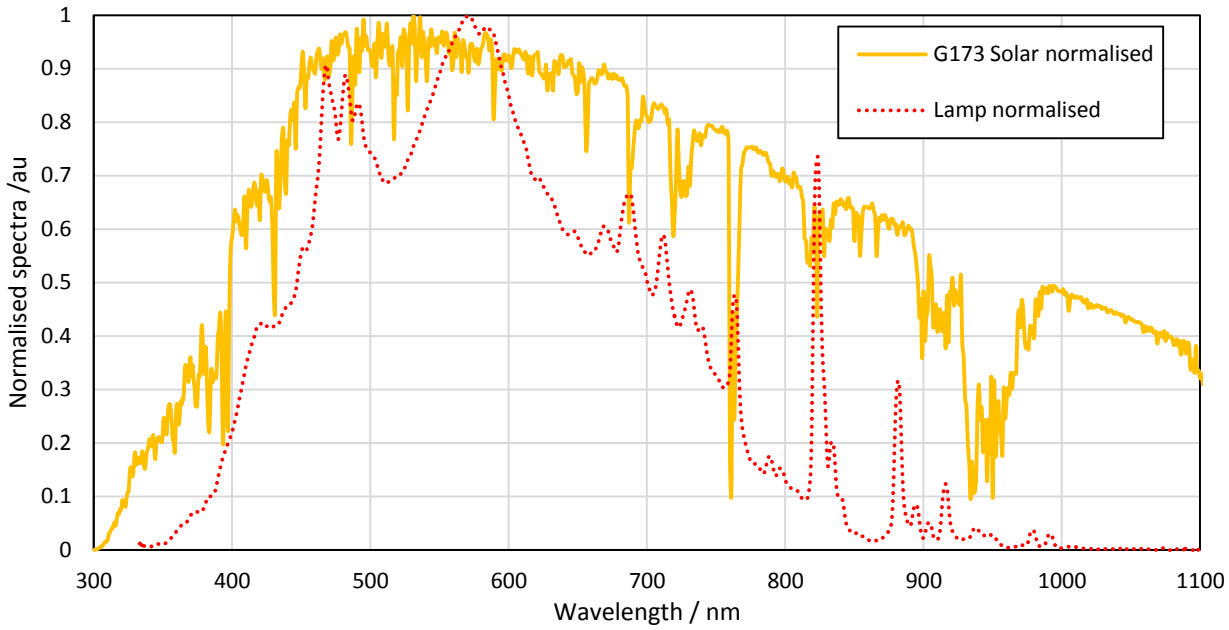

Figure 6 Spectral response of the SSL lamp compared to the G173 solar reference spectra. Both spectra have been normalised for comparison

Using Equation 5, $AE_{Lamp\ (330\text{-}1100\ nm)}$ was calculated from the UV-Vis-IR spectral data for the mixture M and the three component nanofluids. The results are shown in Table 2. Analysis of variance (ANOVA – see SI for details) was undertaken on the data to determine if $AE_{Lamp\ (330\text{-}1100\ nm)}$ for the mixture M was greater than the three nanofluids used for the mixture and to estimate the likely range of the value at a 95% confidence interval. The $AE_{Lamp\ (330\text{-}1100\ nm)}$ of the mixture was greater than 90% showing the potential of this blended nanofluid for solar applications.

Table 2 Results of calculating $AE_{Lamp\ (330\text{-}1100\ nm)}$ *from the UV-Vis-IR data.*

Nanofluid type	**n***	**Grouping**	**Mean $AE_{Lamp\ (330\text{-}1100\ nm)}$ / %**	**Standard deviation (StDev) / %**	**95% confidence interval (CI) for the mean**
P-A	9	B	57.81	1.78	56.01 – 59.62
P-B	9	C	73.97	2.02	72.17 – 75.78
P-C	9	D	46.29	4.61	44.49 – 48.10
M	12	A	92.75	1.37	91.18 – 94.31

** n = number of measurements. The initial, after 4 weeks storage and after exposure to SSL for 30 minutes has been used giving n = 9. In addition for M the calculated spectral data has been included (hence for M, n = 12). Means that do not share the same letter are significantly different (see analysis of variance section in SI)*

Using the actual reference solar spectrum over the extended wavelength range of 300-1350 nm (Equation 3) gives a better indication of the potential performance of the broadband mixture M in sunlight. It should be noted that, although the AE value of mixture M appeared to be greater than 80% (see SI Table S15), it was based on the assumption that all the energy from the solar spectrum outside of the 300 -1350 nm range was absorbed. Therefore, the actual performance of the broadband absorber is likely to be slightly below 80%. Nevertheless, this performance is still impressive for a very dilute nanofluid, showing the benefit of both utilising a plasmonic nanofluid and tailoring the response of that nanofluid by varying the nanoparticle geometry in the fluid to closely match the solar spectra. It should also be noted that all these calculations were undertaken using a light path length of 10 mm. If the path length or the concentration of M was increased, the performance of this blended nanofluid could be further improved. On the other hand, increasing the concentration may, have a detrimental effect on the colloidal stability. Conversely, reducing the nanofluid concentration would potentially improve colloidal stability, but a greater depth of nanofluid would be needed to give the same performance. This would require further investigation.

3.4 Thermal performance of nanofluids under SSL

The thermal performance of nanofluids subject to SSL exposure was measured by monitoring the temperature rise over a period of 10 minutes. The measured temperature profiles on exposure to SSL for the three component nanofluids and the blended broadband mixture are shown in Figure 7, along with the profile for water. The initial temperature recorded at the start of each experiment was 25.7 °C (StDev 0.6 °C N = 39). The nanofluids all exhibited an initial linear temperature rise with time, followed by a decrease in the rate of temperature rising. The trend indicated that, if the time of the experiments was extended, the temperature profile would level out as the stagnation temperature was reached (i.e. the rate of heat loss became equal to the rate of heat gain).

As shown in Equation 4, with a given absorber and irradiation source, the thermal performance is determined by $\Delta T/\Delta t$, the initial slope of the linear temperature rise. Therefore, for these experiments it was not deemed necessary to continue the experiment beyond the linear rise stage, or until the saturation temperature was reached. In addition, if care had not been taken to maintain a consistent starting temperature of the nanofluid, there may have been some variation in the length of the linear portion of the graph, requiring that the slope was calculated over a smaller Δt. However, it should not greatly affect the value of PE obtained (especially when the experimental uncertainties of 8.24 – 10.37 % are considered), unless a significantly higher starting temperature at or near the stagnation temperature was used leading to no linear region on the graph. Further investigation of the effect of starting temperature would be needed to confirm this.

All of the nanofluids exhibited a significantly greater ΔT than water with the M nanofluids showing the largest increase, followed by P-B, P-A and then P-C, in line with the order observed for absorption efficiency $AE_{Lamp\ (330\text{-}1100\ nm)}$. By using the $\Delta T/\Delta t$ values (Figure 7), PE_{Total} values for all four samples were obtained. The results summarised in Table 3, show good agreement with the values obtained for $AE_{Lamp\ (330\text{-}1100\ nm)}$ (Table 2). This is especially valid when the measurement uncertainties of 8.24 – 10.37 % (Section 2.5) are taken into consideration.

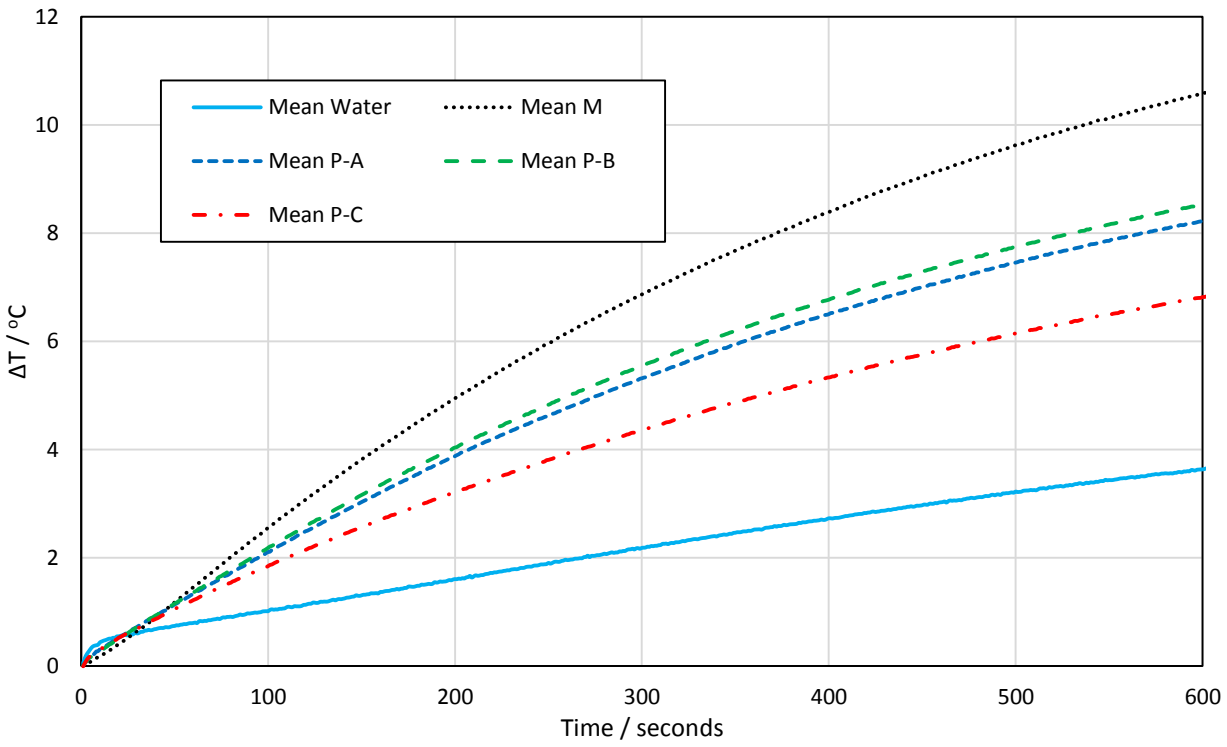

Figure 7 Change in temperature with time of exposure to SSL for the mixture M and components P-A, P-B and P-C. The mean results from 9 measurements per sample type are shown except for water where n = 3

Table 3 Calculated values of PE_{Total} obtained from SSL testing. ANOVA testing (See SI) was undertaken to determine the significance of the results and to determine the possible range of the mean values (at 95% CI). Samples that do not share the same letter are significantly different

Nanofluid type	n*	Grouping	Mean PE_{Total} from SSL / %	StDev / %	95% CI for the mean
Water	3	D	20.51	1.17	14.61 – 26.34
M	9	A	83.77	2.29	80.40 – 87.14
P-A	9	B	62.46	4.49	59.09 – 65.83
P-B	9	B	65.05	7.58	61.68 – 68.42
P-C	9	C	47.68	4.68	44.31 – 51.05

** Number of repeated measurements.*

As discussed above, there is no direct comparison between the results obtained here and those with a blended mixture of gold by Jeon et al (Jeon et al., 2016) who used extinction coefficients for calculation under different conditions, such as using a computer model to calculate efficiency under flow conditions based on static experimental data. Interestingly, their blended gold absorber appeared to give a comparable level of maximum efficiency at about 80-85 %, which is similar to the results obtained in this study (83.77%).

In addition, the silver nanofluid with the two absorption peaks produced by Walshe et al (essentially a mixture with an absorbance covering the range 300 -750 nm) also gave a PE value of about 90%, similar to this study. These results were also obtained from static testing while using different sample geometry and testing protocol. The numerical study by Mallah et al (Mallah et al., 2018) produced better results for efficiency than this study at a lower concentration but with a longer path length employed (up to 98 % for a 10 cm path length). The absorption obtained in the near IR range was better for the nanofluid they proposed containing silver nanorods. To give a true comparison to this work a five component nanofluid with the same concentrations, nanoparticle types and ratio of components would need to be synthesised and tested using the same geometry as they proposed. In fact in their conclusions they acknowledge the importance of conducting experimental studies on these blended nanofluids.

3.5 Characterisation of nanofluids after SSL

To assess the stability of nanofluids subject to light exposure, they were examined with both UV-Vis-IR spectroscopy and TEM following exposure to SSL for 30 minutes for the mixture and three component nanofluids. It was found that there were some changes in the spectra (Figure 8). λ_{max} for nanofluid P-A had blue shifted by approximately 50 nm with a small but significant drop of 5% in H_{peak} (SI Table S16). Nanofluid P-B exhibited a greater blue shift of about 90 nm in λ_{max} with an increase of about 9% in H_{peak}. Nanofluid P-C showed a slight red shift in λ_{max} (see Table S17) but a significant increase of 45 % in H_{peak}. The mixture M also exhibited this significant increase in H_{peak} for the primary peak, mainly due to the contribution of P-C to the spectra. The shape of the spectra for M also changed due to the blue shift in λ_{max} of both P-A and P-B.

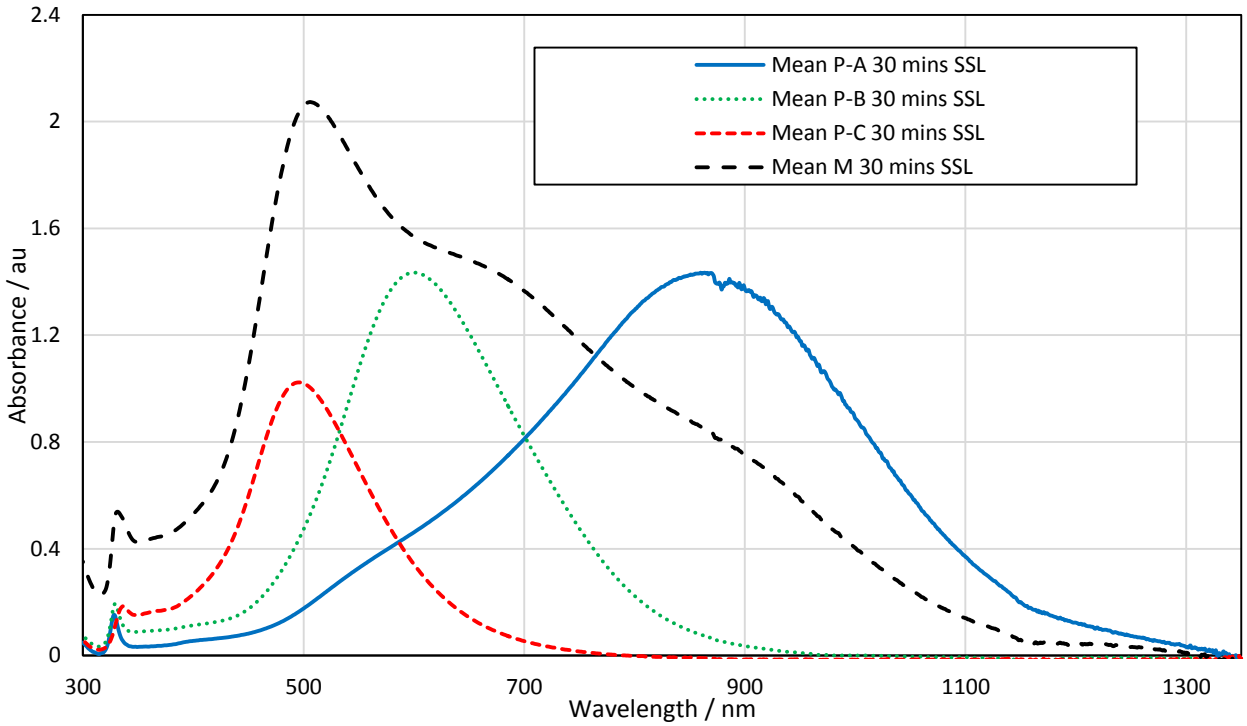

Figure 8 UV-Vis-IR spectra for M, P-A, P-B and P-C after 30 minutes exposure to SSL. Mean values shown. Note that P-B was diluted 1 mL in 3 mL, P-C was diluted 0.6 mL in 3 mL. All measurements undertaken with a 10 mm path length cuvette.

TEM images of P-A, P-B, P-C and the mixture M after SSL are shown in Figure 9. A more detailed size analysis is presented in SI Table S18. It was found that the triangles in sample P-A became more rounded, and in P-B the rounded triangles were even further rounded and mixed with disc-

shaped. To confirm the hypothesis that the disc-shaped particles were derived from the triangles, the percentage of each type of particles was estimated, and the results are shown in Figure 10. As can be seen, the number of rounded corner triangles increased for P-A and the number of other shaped particles (discs and hexagons) increased for P-B. The average size and thicknesses of the particles appeared to be unchanged (Table S18). Hence, the predominate mechanism for this change was believed to be the rounding of the sharp corners of the triangles in P-A, causing a blue shift in the UV-Vis-IR spectra, while a further rounding of the already rounded corner triangles in P-B to more disc-shaped particles. This losing of the sharp corners of silver nanoprisms has been observed previously by others, largely associated with the mechanical and physiochemical properties of the sharp tips (Roh et al., 2012; Tang et al., 2013; Taylor et al., 2018).

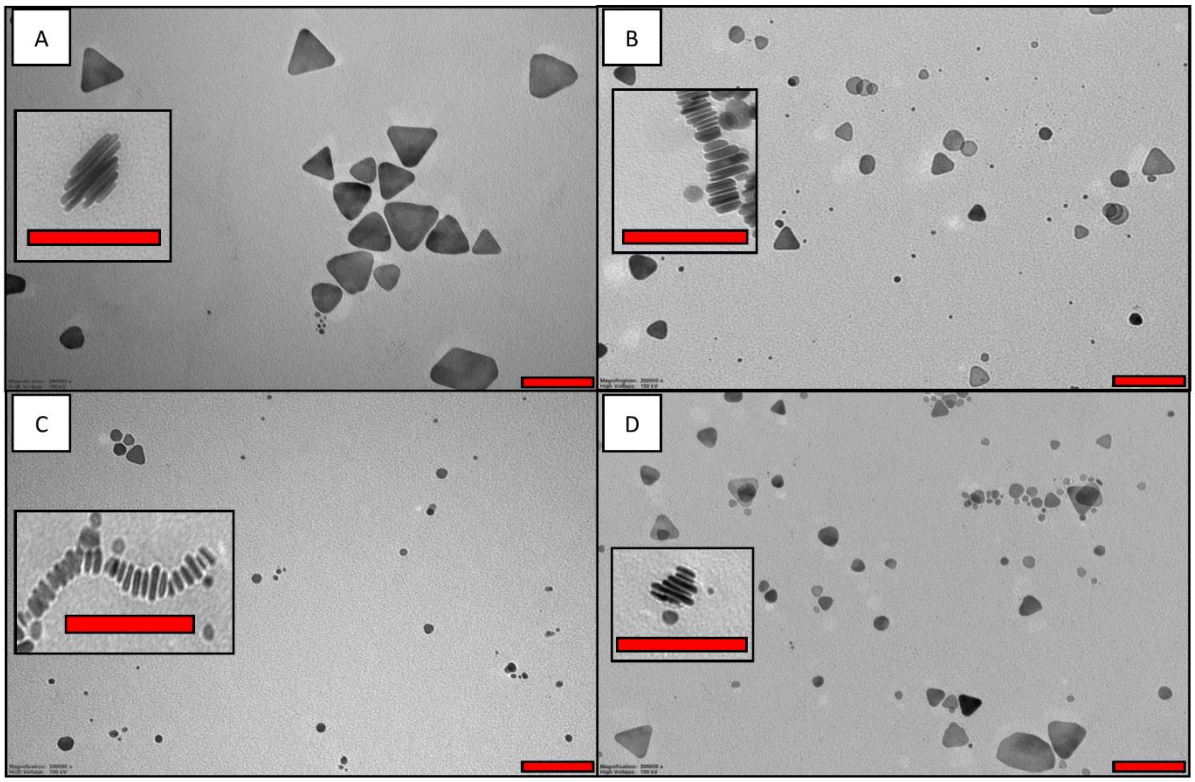

Figure 9 TEM images of A) P-A, B) P-B, C) P-C and D) M after solar simulator testing. The magnified inserts show the edges of the nanoparticles. All scale bars All scale bars including the ones in the inserts = 100 nm

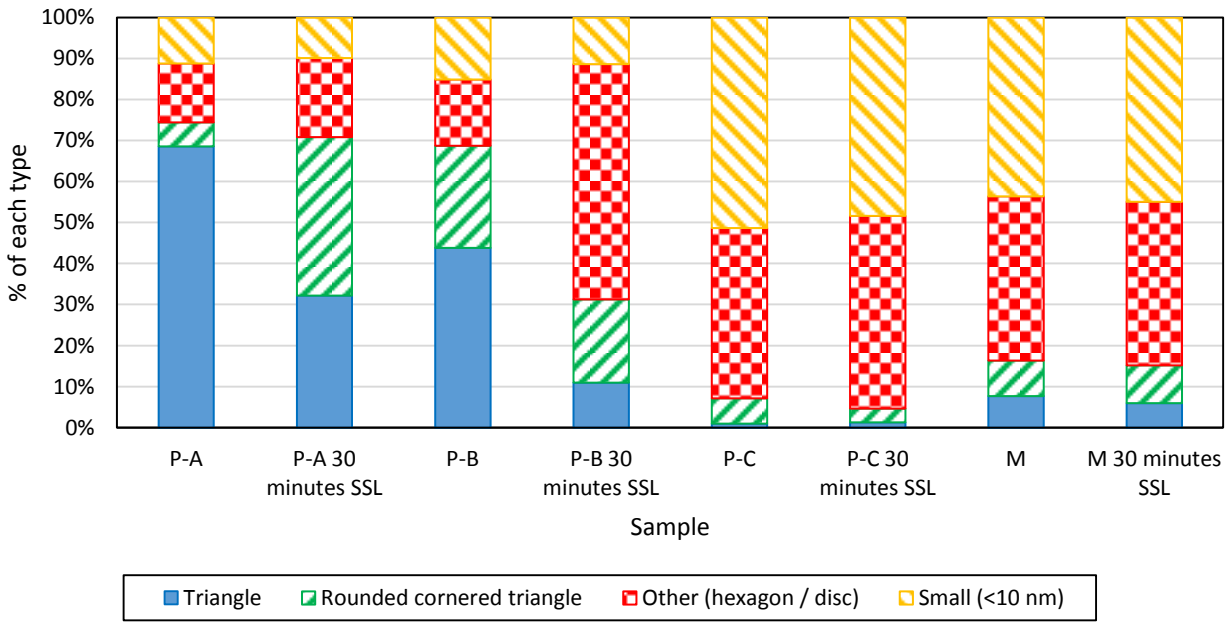

Figure 10 Percentage of each type of particle before and after SSL exposure estimated from TEM micrographs for P-A, P-B, P-C and M

There are a number of potential ways to reduce the instability of silver nanofluids towards photo-induced shape change. The modification of the pH of the nanofluid has been proposed with the addition of OH^- ions (Roh et al., 2012). Coating the silver nanoparticle with e.g. SiO_2 has been explored (Hjerrild et al., 2018; Taylor et al., 2018). This is also an ongoing active research topic in our laboratories (Kimpton et al., 2020).

4 CONCLUSIONS AND FURTHER WORK

For the first time a silver nanofluid-based broadband absorber consisting of three different nanoparticles was produced, and its potential for enhancing solar thermal capture was demonstrated experimentally towards application in direct absorption solar collectors (DASCs). A batch process was used to consistently synthesise three different silver nanofluids with absorption peaks in the ranges 880 -980 nm, 650-750 nm and 450 -520 nm, respectively, just by variation in the amount and timing of the chemical additions. The potential absorption efficiency (AE) was calculated from UV-Vis-IR spectra, and the computed value was compared to the value obtained by measuring real time temperature rise of the nanofluids in a solar simulator.

Comparable results were obtained through the two approaches, i.e. by estimating an average absorption efficiency $AE_{Lamp\ (330\text{-}1100\ nm)}$ with the UV-Vis-IR method (92.75 ± 1.37%), and an average photo-thermal conversion efficiency PE_{Total} of 83.77 ± 2.29 % using the solar simulator method. The similarity of the results obtained enables calculations based on UV-Vis-IR measurements to be used with confidence for the rapid identification and screening of nanofluids for their potential in DASC applications.

Although the nanofluids and mixture were shown to have good colloidal stability after storage in the dark for 4 weeks at 4°C, the story was not the same following light exposure. Subjected to simulated sunlight exposure, the nanoparticles showed a change in absorption spectra and morphology even after only 30 minutes exposure. This is additional information directly confirmed by TEM imaging, but not by the initial UV-Vis-IR spectroscopy. This clearly demonstrates the value of utilising complementary techniques for the assessment of a nanofluids suitability for DASC applications. Although the results presented here are limited to the specific nanofluids tested, they provide useful guidelines for other researchers in determining suitable assessment techniques for their nanofluids.

Due to the instability of the silver nanofluids shown here, a suitable coating or stabilisation strategy would be required for further development of this broadband absorber for solar energy capture applications. Nonetheless, compared to the timeframe of conventional surface-based solar collectors (i.e. 20 years), it will still be challenging to make a silver-based nanofluid for long-term running in the harsh environmental conditions experienced. This lack of long-term stability has been muted as one of the reasons hindering DASCs commercialisation (Sharaf et al., 2019).

Further work will firstly focus on the effect of temperature alone on the broadband absorber stability as it is important to determine if the instability is due to the solar radiation or a combination of solar radiation and heat. The focus will then shift to measuring the broadband absorber under flow conditions to get a better understanding of potential performance and stability to mechanical damage. After this, methods of stabilising the silver morphology will be investigated in the hope that the broadband absorber developed here could be made more suitable for solar energy applications.

5 ACKNOWLEDGEMENTS

The authors acknowledge the support of the EPSRC-funded CDT in Energy Storage and Its Applications and the Faculty of Engineering and Physical Sciences both at the University of Southampton. They would especially like to thank Thomas Mercier for his assistance with the lamp intensity measurements using the ReRA system calibrated PV cell, and Associate Professor Dmitry Bavykin and Professor Andrew Cruden for their valuable discussions.

6 REFERENCES

Abdelrazik, A.S., Al-Sulaiman, F.A., Saidur, R., 2019. Optical behavior of a water/silver nanofluid and their influence on the performance of a photovoltaic-thermal collector. Solar Energy Materials and Solar Cells, 201, 110054, https://doi.org/10.1016/j.solmat.2019.110054.

Aherne, D., Ledwith, D.M., Gara, M., Kelly, J.M., 2008. Optical Properties and Growth Aspects of Silver Nanoprisms Produced by a Highly Reproducible and Rapid Synthesis at Room Temperature. Advanced Functional Materials, 18(14), 2005-2016, https://doi.org/10.1002/adfm.200800233.

Ahmad, S.H.A., Saidur, R., Mahbubul, I.M., Al-Sulaiman, F.A., 2017. Optical properties of various nanofluids used in solar collector: A review. Renewable and Sustainable Energy Reviews, 73, 1014-1030, https://doi.org/10.1016/j.rser.2017.01.173.

ASTM, 2012. Reference Solar Spectral Irradiance: ASTM G-173. https://rredc.nrel.gov/solar//spectra/am1.5/ASTMG173/ASTMG173.html. (Accessed 01 July 2019.

Bandarra Filho, E.P., Mendoza, O.S.H., Beicker, C.L.L., Menezes, A., Wen, D., 2014. Experimental investigation of a silver nanoparticle-based direct absorption solar thermal system. Energy Conversion and Management, 84, 261-267, https://doi.org/10.1016/j.enconman.2014.04.009.

Bastys, V., Pastoriza-Santos, I., Rodríguez-González, B., Vaisnoras, R., Liz-Marzán, L.M., 2006. Formation of Silver Nanoprisms with Surface Plasmons at Communication Wavelengths. Advanced Functional Materials, 16(6), 766-773, https://doi.org/10.1002/adfm.200500667.

Bell, S., 2001. A Beginner's Guide to Uncertainty of Measurement. NPL, UK TW11 0LW, https://www.dit.ie/media/physics/documents/GPG11.pdf. (Accessed 20 November 2019).

Carboni, M., Capretto, L., Carugo, D., Stulz, E., Zhang, X., 2013. Microfluidics-based continuous flow formation of triangular silver nanoprisms with tuneable surface plasmon resonance. Journal of Materials Chemistry C, 1(45), 7540, https://doi.org/10.1039/c3tc31335b.

Carboni, M., Carravetta, M., Zhang, X.L., Stulz, E., 2016. Efficient NIR light blockage with matrix embedded silver nanoprism thin films for energy saving window coating. J. Mater. Chem. C, 4(8), 1584-1588, https://doi.org/10.1039/c6tc00026f.

Chen, M., He, Y., Zhu, J., Wen, D., 2016. Investigating the collector efficiency of silver nanofluids based direct absorption solar collectors. Applied Energy, 181, 65-74, https://doi.org/10.1016/j.apenergy.2016.08.054.

Crisostomo, F., Hjerrild, N., Mesgari, S., Li, Q., Taylor, R.A., 2017. A hybrid PV/T collector using spectrally selective absorbing nanofluids. Applied Energy, 193, 1-14, https://doi.org/10.1016/j.apenergy.2017.02.028.

Du, M., Tang, G.H., 2016. Plasmonic nanofluids based on gold nanorods/nanoellipsoids/nanosheets for solar energy harvesting. Solar Energy, 137, 393-400, https://doi.org/10.1016/j.solener.2016.08.029.

Duffie, J.A., Beckman, W.A., 2013. Solar Engineering of Thermal Processes, Fourth Edition. John Wiley & Sons.

Engineering Toolbox, 2004. Water - Specific Heat. https://www.engineeringtoolbox.com/specific-heat-capacity-water-d_660.html. (Accessed 21 January 2020.

Goel, N., Taylor, R.A., Otanicar, T., 2020. A review of nanofluid-based direct absorption solar collectors: Design considerations and experiments with hybrid PV/Thermal and direct steam generation collectors. Renewable Energy, 145, 903-913, https://doi.org/10.1016/j.renene.2019.06.097.

Gorji, T.B., Ranjbar, A.A., 2015. Geometry optimization of a nanofluid-based direct absorption solar collector using response surface methodology. Solar Energy, 122, 314-325, https://doi.org/10.1016/j.solener.2015.09.007.

Gorji, T.B., Ranjbar, A.A., 2016. A numerical and experimental investigation on the performance of a low-flux direct absorption solar collector (DASC) using graphite, magnetite and silver nanofluids. Solar Energy, 135, 493-505, https://doi.org/10.1016/j.solener.2016.06.023.

Gorji, T.B., Ranjbar, A.A., 2017. A review on optical properties and application of nanofluids in direct absorption solar collectors (DASCs). Renewable and Sustainable Energy Reviews, 72, 10-32, https://doi.org/10.1016/j.rser.2017.01.015.

Gupta, H.K., Agrawal, G.D., Mathur, J., 2015. Experimental Evaluation of Using Nanofluid in Direct Absorption Solar Collector, Energy Technology & Ecological Concerns: A Contemporary Approach. 150-154.

Haber, J., Sokolov, K., 2017. Synthesis of Stable Citrate-Capped Silver Nanoprisms. Langmuir, 33(40), 10525-10530, https://doi.org/10.1021/acs.langmuir.7b01362.

Hjerrild, N.E., Scott, J.A., Amal, R., Taylor, R.A., 2018. Exploring the effects of heat and UV exposure on glycerol-based Ag-SiO_2 nanofluids for PV/T applications. Renewable Energy, 120, 266-274, https://doi.org/10.1016/j.renene.2017.12.073.

Iyahraja, S., Rajadurai, J.S., 2015. Study of thermal conductivity enhancement of aqueous suspensions containing silver nanoparticles. AIP Advances, 5(5), 057103, https://doi.org/10.1063/1.4919808.

Jeon, J., Park, S., Lee, B.J., 2014. Optical property of blended plasmonic nanofluid based on gold nanorods. Opt Express, 22 Suppl 4, A1101-1111, https://doi.org/10.1364/OE.22.0A1101.

Jeon, J., Park, S., Lee, B.J., 2016. Analysis on the performance of a flat-plate volumetric solar collector using blended plasmonic nanofluid. Solar Energy, 132, 247-256, https://doi.org/10.1016/j.solener.2016.03.022.

Jin, H., Lin, G., Bai, L., Amjad, M., Bandarra Filho, E.P., Wen, D., 2016. Photothermal conversion efficiency of nanofluids: An experimental and numerical study. Solar Energy, 139, 278-289, https://doi.org/10.1016/j.solener.2016.09.021.

Kazemi-Beydokhti, A., Heris, S.Z., Moghadam, N., Shariati-Niasar, M., Hamidi, A.A., 2014. Experimental Investigation of Parameters Affecting Nanofluid Effective Thermal Conductivity. Chemical Engineering Communications, 201(5), 593-611, https://doi.org/10.1080/00986445.2013.782291.

Khullar, V., Tyagi, H., Hordy, N., Otanicar, T.P., Hewakuruppu, Y., Modi, P., Taylor, R.A., 2014. Harvesting solar thermal energy through nanofluid-based volumetric absorption systems.

International Journal of Heat and Mass Transfer, 77, 377-384, https://doi.org/10.1016/j.ijheatmasstransfer.2014.05.023.

Kimpton, H., Cristaldi, D.A., Stulz, E., Zhang, X., 2020. Thermal performance and physicochemical stability of silver nanoprism-based nanofluids for direct solar absorption. Solar Energy, 199, 366-376, https://doi.org/10.1016/j.solener.2020.02.039.

Ledwith, D.M., Whelan, A.M., Kelly, J.M., 2007. A rapid, straight-forward method for controlling the morphology of stable silver nanoparticles. Journal of Materials Chemistry, 17(23), 2459, https://doi.org/10.1039/b702141k.

Lee, S.Y., Jin, S.H., Kim, S.M., Kim, J.W., 2016. Solution plasma process to synthesize silver nanofluids and their thermal conductivity behaviors. Metals and Materials International, 20(4), 695-699, https://doi.org/10.1007/s12540-014-4014-1.

Luo, Z., Wang, C., Wei, W., Xiao, G., Ni, M., 2014. Performance improvement of a nanofluid solar collector based on direct absorption collection (DAC) concepts. International Journal of Heat and Mass Transfer, 75, 262-271, https://doi.org/10.1016/j.ijheatmasstransfer.2014.03.072.

Mabey, T., Andrea Cristaldi, D., Oyston, P., Lymer, K.P., Stulz, E., Wilks, S., William Keevil, C., Zhang, X., 2019. Bacteria and nanosilver: the quest for optimal production. Crit Rev Biotechnol, 39(2), 272-287, https://doi.org/10.1080/07388551.2018.1555130.

Mallah, A.R., Kazi, S.N., Zubir, M.N.M., Badarudin, A., 2018. Blended morphologies of plasmonic nanofluids for direct absorption applications. Applied Energy, 229, 505-521, https://doi.org/10.1016/j.apenergy.2018.07.113.

Minardi, J.E., Chuang, H.N., 1975. Performance of a "black" liquid flat-plate solar collector. Solar Energy, 17(3), 179-183, https://doi.org/https://doi.org/10.1016/0038-092X(75)90057-2.

Modest, M., 2003. Radiative Heat transfer, 2nd Edition ed. Academic press, USA.

Nasrin, R., Parvin, S., Alim, M.A., 2015. Heat Transfer and Collector Efficiency through a Direct Absorption Solar Collector with Radiative Heat Flux Effect. Numerical Heat Transfer, Part A: Applications, 68(8), 887-907, https://doi.org/10.1080/10407782.2015.1023122.

Otanicar, T.P., Golden, J.S., 2009. Comparative Environmental and Economic Analysis of Conventional and Nanofluid Solar Hot Water Technologies. Environ Sci Technol, 43, 6032-6037.

Otanicar, T.P., Phelan, P.E., Golden, J.S., 2009. Optical properties of liquids for direct absorption solar thermal energy systems. Solar Energy, 83(7), 969-977, https://doi.org/10.1016/j.solener.2008.12.009.

Otanicar, T.P., Phelan, P.E., Prasher, R.S., Rosengarten, G., Taylor, R.A., 2010. Nanofluid-based direct absorption solar collector. Journal of Renewable and Sustainable Energy, 2(3), 033102, https://doi.org/10.1063/1.3429737.

Roh, J., Umh, H.N., Sung, H.K., Lee, B.-c., Kim, Y., 2012. Repression of photomediated morphological changes of silver nanoplates. Colloids and Surfaces A: Physicochemical and Engineering Aspects, 415, 449-453, https://doi.org/10.1016/j.colsurfa.2012.09.018.

Sharaf, O.Z., Rizk, N., Joshi, C.P., Abi Jaoudé, M., Al-Khateeb, A.N., Kyritsis, D.C., Abu-Nada, E., Martin, M.N., 2019. Ultrastable plasmonic nanofluids in optimized direct absorption solar collectors. Energy Conversion and Management, 199, https://doi.org/10.1016/j.enconman.2019.112010.

Sheffield Hallam University, 2019. Beer's Law. https://teaching.shu.ac.uk/hwb/chemistry/tutorials/molspec/beers1.htm. (Accessed 09 October 2019.

Tang, B., Xu, S., An, J., Zhao, B., Xu, W., 2009. Photoinduced Shape Conversion and Reconstruction of Silver Nanoprisms. J. Phys. Chem C, 113, 7025-7030.

Tang, B., Xu, S., Hou, X., Li, J., Sun, L., Xu, W., Wang, X., 2013. Shape evolution of silver nanoplates through heating and photoinduction. ACS Appl Mater Interfaces, 5(3), 646-653, https://doi.org/10.1021/am302072u.

Taylor, R.A., Hjerrild, N., Duhaini, N., Pickford, M., Mesgari, S., 2018. Stability testing of silver nanodisc suspensions for solar applications. Applied Surface Science, 455, 465-475, https://doi.org/10.1016/j.apsusc.2018.05.201.

Turkyilmazoglu, M., 2016. Performance of direct absorption solar collector with nanofluid mixture. Energy Conversion and Management, 114, 1-10, https://doi.org/10.1016/j.enconman.2016.02.003.

Tyagi, H., Phelan, P., Prasher, R., 2009. Predicted Efficiency of a Low-Temperature Nanofluid-Based Direct Absorption Solar Collector. Journal of Solar Energy Engineering, 131(4), 041004, https://doi.org/10.1115/1.3197562.

Walshe, J., Amarandei, G., Ahmed, H., McCormack, S., Doran, J., 2019. Development of poly-vinyl alcohol stabilized silver nanofluids for solar thermal applications. Solar Energy Materials and Solar Cells, 201, https://doi.org/10.1016/j.solmat.2019.110085.

Xu, G., Chen, W., Deng, S., Zhang, X., Zhao, S., 2015. Performance Evaluation of a Nanofluid-Based Direct Absorption Solar Collector with Parabolic Trough Concentrator. Nanomaterials, 5(4), 2131-2147, https://doi.org/10.3390/nano5042131.

Zhang, Q., Li, N., Goebl, J., Lu, Z., Yin, Y., 2011. A systematic study of the synthesis of silver nanoplates: is citrate a "magic" reagent? J Am Chem Soc, 133(46), 18931-18939, https://doi.org/10.1021/ja2080345.

Zmijan, R., Carboni, M., Capretto, L., Stulz, E., Zhang, X., 2014. In situ microspectroscopic monitoring within a microfluidic reactor. RSC Adv., 4(28), 14569-14572, https://doi.org/10.1039/c4ra01650e.

Supplementary information Marked-Revision

Click here to download Electronic Annex: SI Broadband paper Kimpton SE-D-20-01506 R1.docx

Silver nanofluids based broadband solar absorber through tuning nanosilver geometries

Highlights

- Three silver-based nanofluids combined to give a broadband solar absorber
- Each with distinct morphology and tailored plasmonic response
- Potential efficiency evaluated experimentally for volumetric absorption
- Enhanced photo-conversion efficiency of ≈ 85% achieved
- Static solar simulator results comparable to UV-vis-IR efficiency estimations

Graphical Abstract (for review)

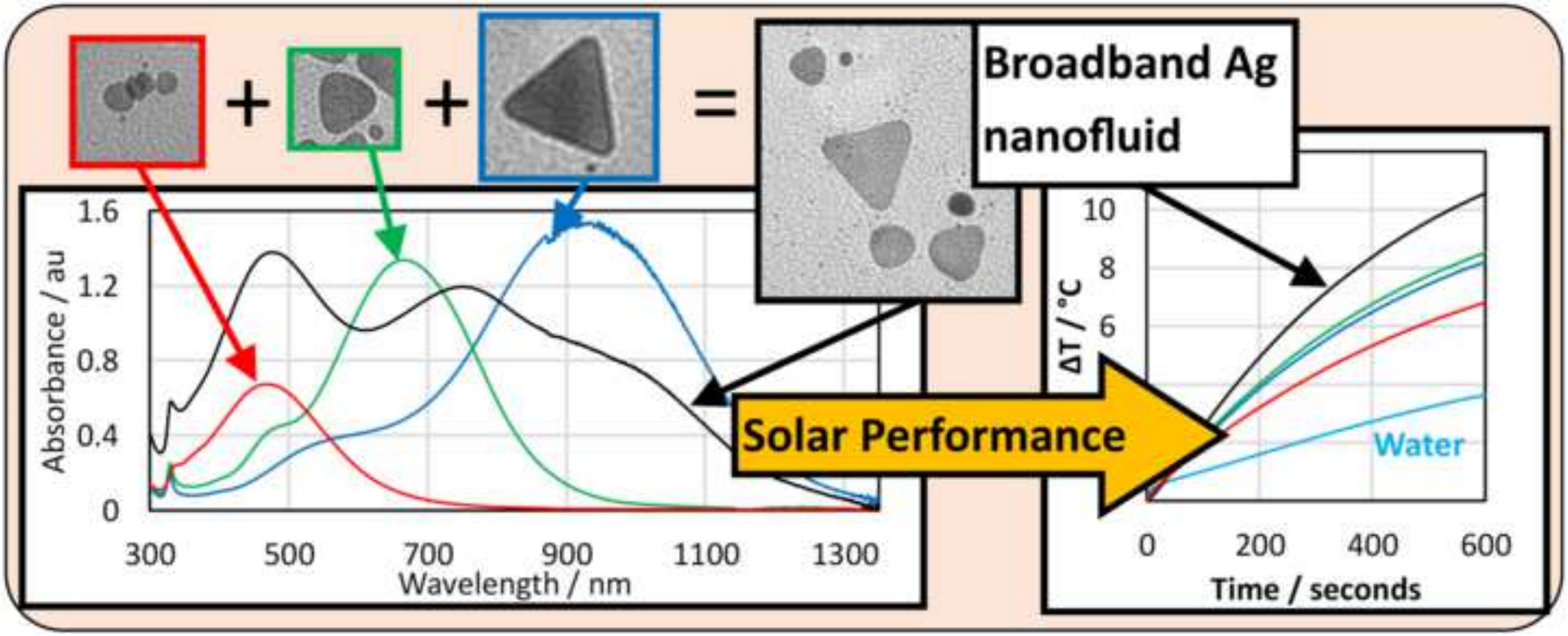

*Unmarked Revised Manuscript For Publication
Click here to view linked References

Silver nanofluids based broadband solar absorber through tuning nanosilver geometries

Harriet Kimpton[ab], Eugen Stulz[a*], Xunli Zhang[b*]

[a] *School of Chemistry, University of Southampton, University Road, Southampton, SO17 1BJ, UK*

[b] *School of Engineering, University of Southampton, University Road, Southampton, SO17 1BJ, UK*

** Corresponding Authors: X. Zhang (XL.Zhang@soton.ac.uk); E. Stulz (est@soton.ac.uk)*

ABSTRACT

This work explores the strategy for increasing the efficiency of solar thermal energy capture by the utilisation of a blended mixture of plasmonic silver nanofluids in a direct absorption solar collector. For the first time, a broadband absorber based on combining three silver-based nanofluids, each with a tailored plasmonic response covering a different wavelength range, was designed and synthesised. The potential efficiency of this broadband absorber was estimated from the UV-Vis-IR spectra and from direct measurement of the temperature rise obtained in static tests in a solar simulator. The results from the two methods were comparable. The broadband absorber was shown to increase the efficiency of capture compared to the component nanofluids and compared to water. The temperature rise in the solar simulator for the broadband mixture was more than four times that of water and the photo-thermal conversion efficiency was approximately 85%, demonstrating the promise of this mixture for enhancing solar energy capture. However, this work also illustrates the potential issues with utilising silver for solar applications, namely the change in morphology and UV-Vis-IR spectra with light exposure. A suitable stabilisation or coating strategy would hence be required to use this developed broadband absorber in solar energy applications.

Keywords: Nanofluids; Plasmonic; Broadband solar absorber; Stability; Silver nanoprisms; Silver nanodiscs

Author declaration: This publication has no known conflicts of interest. Its outcome was not influenced significantly by any financial support.

Abbreviations:

AE	Absorption efficiency / %
A_s	Surface area
AgNPs	Silver nanoparticles
ANOVA	Analysis of variance
A_λ	Absorption at wavelength λ
CI	Confidence interval
C_w	Base-fluid heat capacity / Jkg^{-1} K^{-1}
DASC	Direct absorption solar collector
H_{Peak}	Height of maximum absorption peak / au
IR	Infra-red
I_s	Incident radiative intensity / Wm^{-2}
M	Mixture
M_w	Base-fluid mass / kg
$P_{Ab(\lambda)}$	Power absorbed at wavelength λ / Wm^{-2}
PE_{Total}	Total photo-thermal conversion efficiency / %
$P_{i(\lambda)}$	Incident power intensity at λ / Wm^{-2}
$P_{T(\lambda)}$	Power transmitted at wavelength λ / Wm^{-2}
PVP	Polyvinylpyrrolidone
SI	Supplementary information
SSL	Simulated sunlight
StDev	Standard deviation
TEM	Transition electron microscopy
TSCD	Tri-sodium citrate dehydrate

UV	Ultraviolet
wks	Week
wt %	weight / %
Δt	Change in time / s
ΔT	Temperature change / °C
λ_{max}	Wavelength of maximum absorption peak / nm

1 INTRODUCTION

Direct absorption solar collectors (DASCs), proposed initially in the 1970's (Minardi and Chuang, 1975), are designed to directly absorb solar thermal energy into a volume of liquid which is also used as the working fluid for subsequent heat transfer. Compared to the traditional selective absorbing surface collectors (Gupta et al., 2015) DASCs have a number of advantages, namely, simpler manufacturing, improved heat transfer and reduced heat loss due to an even temperature distribution in the fluid (Iyahraja and Rajadurai, 2015; Lee et al., 2016; Luo et al., 2014; Otanicar and Golden, 2009; Otanicar et al., 2010; Tyagi et al., 2009; Xu et al., 2015). These factors have led to an overall increase in collector efficiency of about 10% (Nasrin et al., 2015; Turkyilmazoglu, 2016).

However, without additions the working fluids employed in most DASCs only absorb a low percentage of the solar radiation in the range of 2% to 14% over the wavelength range 200 - 1500 nm (Otanicar et al., 2009). This can be overcome by the addition of Indian ink or micro particulate carbon (Gorji and Ranjbar, 2016) but the addition of large particles can cause issues with sedimentation, erosion and pump blockages (Kazemi-Beydokhti et al., 2014; Khullar et al., 2014). Hence, in recent years there has been considerable interest in the use of nanoparticles to engineer colloidal nanofluids with superior absorption characteristics, small particle sizes and low concentrations. In this aspect, metallic nanoparticles that exhibit surface plasmonic resonance at certain wavelengths can improve absorption characteristics while maintaining a very low

nanoparticle concentration, and improving colloidal stability (Ahmad et al., 2017; Du and Tang, 2016).

The plasmonic response of metallic nanoparticles only occurs at certain wavelengths, depending on the shape and size of the particles used, thus leading to narrow spectra absorption. To overcome this limitation a blend of different plasmonic nanoparticles can be used as a broadband absorber with enhanced absorption at low nanoparticle concentration. For example, blended gold nanorods with different aspect ratios (Jeon et al., 2014; Jeon et al., 2016) and mixtures of gold nanorods with ellipsoids and nanosheets (Du and Tang, 2016) have been studied as plasmonic broadband absorbers for DASC and other solar applications. A blended nanofluid has been concepted as the ideal broadband solar absorber for DASC applications (Goel et al., 2020; Sharaf et al., 2019), and two silver broadband mixtures comprising five different silver nanoparticle geometries have been investigated numerically (Mallah et al., 2018). Their two blended nanofluids gave absorption efficiencies of 98 % and 95 % respectively over the range of 300-2500 nm for a nanofluid depth of 10 cm. This work complements this numerical work, using a simpler three component mixture, but provides additional information on issues that occur when mixtures of different nanoparticle geometries are combined together experimentally. The concept of a broadband absorber based on silver is not novel, but to the authors' best knowledge the experimental production and subsequent testing of such a blended broadband absorber mixture has not been reported.

The surface plasmonic response of silver nanoparticles, similar to other metallic particles is highly dependent on the size and shape of the nanoparticles in the nanofluid (Aherne et al., 2008; Haber and Sokolov, 2017; Ledwith et al., 2007). Most experimental studies for DASC applications have focused on nanospheres (Abdelrazik et al., 2019) with a strong absorption around 400 nm and have shown efficiency improvements of between 5 % and 144% (Bandarra Filho et al., 2014; Chen et al., 2016; Otanicar et al., 2010), compared to water. Some work has also been carried out on anisotropic silver nanodiscs with a plasmonic response at about 650 nm for volumetric absorption (Crisostomo et al., 2017; Hjerrild et al., 2018; Taylor et al., 2018). Interestingly, Walshe et al "accidentally" produced a silver nanofluid with two different absorption peaks at approximately 430 and 600 nm which gave a good photo-thermal conversion efficiency (PE) of 70% - 90% depending on nanoparticle concentration (Walshe et al., 2019).

In our series of research on silver nanoparticles, we have focused on producing consistently silver nanoprisms with a strong absorption in the near infra-red (Carboni et al., 2013; Carboni et al., 2016; Mabey et al., 2019; Zmijan et al., 2014). This development has provided us with necessary fundamental understanding and practical tools to design and produce a blended silver broadband absorber consisting of a number of component nanofluids containing different sizes and shapes of silver nanoparticles for desired plasmonic responses. There are a range of methods for controlling the morphology and hence position of the plasmonic absorption for silver nanoparticles, such as photo-mediated methods (Bastys et al., 2006; Tang et al., 2009; Tang et al., 2013) and various chemical methods (both direct and utilising a silver seed solution) (Aherne et al., 2008; Haber and Sokolov, 2017; Ledwith et al., 2007). In the work with a modified direct chemical method (Zhang et al., 2011), the reduction of silver ions were carried out with sodium borohydride in the presence of hydrogen peroxide to give nanoprisms The amount and timing of the addition of the reagents was adjusted to vary the size and shape of the particles produced.

The aim of the present study was to demonstrate the proof-of-principle of utilising a broadband, blended plasmonic absorber for DASC applications based on silver nanofluid. Three types of silver nanofluids with different size and shape of nanoparticles were synthesised with plasmonic responses in the range of 880 - 980 nm, 650 - 750 nm and 450 - 520 nm, respectively. These were blended to give a mixture for broadband solar absorption. The solar performance of individual component nanofluids and their broadband mixture were then assessed by using ultraviolet-visible-infrared (UV-Vis-IR) spectroscopy and a solar simulator, hence providing quantitative evaluation towards solar energy capture applications. This study was designed, for the first time, to create a broadband absorber utilising silver nanoparticles with a tailored absorption profile to match the solar spectrum in the Vis-IR range by physically blending three separate nanofluids. It was also the first time that the performance of this novel nanofluid was investigated in static tests utilising a solar simulator, and further compared with theoretical spectroscopy analysis and calculations.

2 EXPERIMENTAL METHODS

2.1 Chemicals

All chemicals were sourced from Sigma Aldrich. They were used as purchased and consisted of: Sodium borohydride ($NaBH_4$, 99%), hydrogen peroxide (H_2O_2 30 weight percentage (wt.%)), silver nitrate ($AgNO_3$ 99%), Polyvinylpirrolidone (PVP, average molecular weight ≈ 29,000 g mol^{-1}), and tri-sodium citrate dihydrate (TSCD). Milli-Q water was used throughout.

2.2 Synthesis

Procedure A (P-A): This synthesis was designed to produce silver nanoparticles (AgNPs) with absorption maxima (λ_{max}) in the 850 - 950 nm range with a final silver concentration of 0.1 mM Ag. This concentration was chosen based on prior knowledge of ease and consistency of synthesis (SI Table S1). The synthesis was based on that employed by Zhang *et al* (Zhang et al., 2011) with some modifications, where AgNPs were stabilised with both PVP and TSCD (Kimpton et al., 2020). Briefly, 24 mL aqueous solution comprising of hydrogen peroxide (H_2O_2, 30 wt.%, 0.125 mL), silver nitrate ($AgNO_3$, 0.05 M, 0.05 mL), PVP (0.70 mM, 0.375 mL) and TSCD (0.10 M, 0.375 mL) was vigorously agitated at room temperature using a magnetic stirrer for 7 minutes. That was followed by rapidly injecting a newly prepared sodium borohydride solution ($NaBH_4$, 25.00 mM, 1.00 mL). It took another 30 minutes of stirring for the reaction to then proceed via a noticeable colour change with gas evolution, through light yellow to orange, brown-orange, and blue-green and finally to blue over a further period of 5 - 10 minutes.

Three batches of PVP and TSCD stabilised AgNPs (25 mL each) were produced (labelled P-A1, P-A2 and P-A3, respectively). A Perkin Elmer Lambda 750S UV-Vis-IR spectrophotometer was used to acquire the spectra of the batches. A 10 mm light path length cuvette was employed.

Procedure B (P-B): This synthesis was designed to produce AgNPs with absorption maxima in the 650 -700 nm range, with a final silver concentration of 0.3 mM Ag (SI Table S1) again based on prior experimental knowledge to ensure ease and consistency of the reaction. The synthesis employed for Procedure A was adapted by reducing the ratio of sodium borohydride to produce more rounded triangular AgNPs while also increasing the starting concentration of silver, PVP and

TSCD in solution. Briefly, 23.5 mL of solution containing TSCD (0.10 M, 1.125 mL), silver nitrate ($AgNO_3$, 0.05 M, 0.15 mL), PVP (0.70 mM, 1.125 mL) and hydrogen peroxide (H_2O_2, 30 wt.%, 0.375 mL) was stirred vigorously at room temperature. After 7 minutes a freshly prepared solution of sodium borohydride ($NaBH_4$, 25.00 mM, 1.5 mL) was rapidly injected. After about 15 minutes, the solution colour changed rapidly through yellow to orange-brown, then through to green-blue after a further 5 - 10 minutes.

With three 25 mL batches (denoted P-B1, P-B2, and P-B3, respectively) of TSCD and PVP stabilised AgNPs produced, UV-Vis spectra (using a Perkin Elmer Lambda 750S UV-Vis-IR spectrophotometer) of each batch were recorded. The samples were diluted to 1 mL in 3 mL with Milli-Q water prior to measuring the spectra to prevent saturation of the detector and a 10 mm cuvette was employed.

Procedure C (P-C): This synthesis was designed to produce disc-shaped small AgNPs with a λ_{max} of 420 -500 nm, with a final silver concentration of 0.457 mM (SI Table S1). Firstly, AgNPs were synthesised using Procedure B but with half the H_2O_2 amount. These were then used as a starting point to produce smaller AgNP discs by the addition of more silver and reducing agent. Briefly, 23.5 mL of solution containing TSCD (0.10 M, 1.125 mL), silver nitrate ($AgNO_3$, 0.05 M, 0.15 mL), PVP (0.70 mM, 1.125 mL) and hydrogen peroxide (H_2O_2, 30 wt.%, 0.188 mL) was stirred vigorously at room temperature. After 7 minutes a freshly prepared solution of sodium borohydride ($NaBH_4$, 25.00 mM, 1.5 mL) was rapidly injected. After about 15 minutes, the solution colour changed rapidly through yellow to orange-brown, then through to green-blue after a further 5-10 minutes. More silver nitrate ($AgNO_3$, 0.05 M, 0.083 mL) was then added, with vigorous stirring followed by the rapid injection of more sodium borohydride ($NaBH_4$, 25.00 mM, 0.42 mL). Again, with three batches (denoted P-C1, P-C2 and P-C3, respectively) UV-Vis-IR spectroscopy was undertaken. The samples (0.6 mL) were diluted with Milli-Q water to give a total volume of 3.0 mL to prevent saturation of the detector with a 10 mm cuvette employed for the UV-Vis-IR spectroscopy measurement.

Mixture (denoted M): The UV-Vis-IR spectra obtained from P-A, P-B and P-C were used to calculate the best combination of all three components to give as high a percentage coverage of the solar spectra as possible. The solar reference spectra utilised was the direct + circumsolar

spectrum from ASTM G173 (ASTM, 2012). This was used as a reference to calculate how much of the solar spectrum was covered by the mixture.

In physics, from Beer's law, absorption of light is a measure of how matter takes up a photon's energy at a given wavelength λ, that is expressed by the following formula (Khullar et al., 2014; Sheffield Hallam University, 2019):

$$A_\lambda = log_{10} \frac{P_{i(\lambda)}}{P_{T(\lambda)}}$$

Equation 1

where A_λ is the absorption at wavelength λ (au); $P_{i(\lambda)}$ is the incident power intensity at λ in Wm^{-2}; and $P_{T(\lambda)}$ is the power transmitted at wavelength λ (Wm^{-2}). Hence Power absorbed $P_{Ab(\lambda)}$ in Wm^{-2} at a given wavelength is:

$$P_{Ab(\lambda)} = P_{i(\lambda)} - \frac{P_{i(\lambda)}}{10^{A_\lambda}}$$

Equation 2

The absorption efficiency (AE) over the wavelength range (300-1350 nm) is then obtained by dividing the sum of the power absorbed by the sample, $\sum_{\lambda=300}^{\lambda=1350} P_{Ab(\lambda)}$, by the total incident power over the wavelength measured, $\sum_{\lambda=300}^{\lambda=1350} P_{i(\lambda)}$, according to the formula (Du and Tang, 2016; Duffie and Beckman, 2013; Modest, 2003):

$$AE_{(300-1350nm)} = \frac{\sum_{\lambda=300}^{\lambda=1350} P_{Ab(\lambda)}}{\sum_{\lambda=300}^{\lambda=1350} P_{i(\lambda)}} \times 100$$

Equation 3

where $\sum_{\lambda=300}^{\lambda=1350} P_{i(\lambda)}$ = 793.1 Wm^{-2} (taken from the Reference Solar Spectral Irradiance G173 spectra (ASTM, 2012)). It should be noted that the apparatus employed only allowed the measurement of the broadband absorber over the 300 – 1350 nm range which accounts for 88.1% of the power of the total solar spectrum from 280 to 4000 nm. Hence $P_{i(280\text{-}4000nm)}$ = 900.2 Wm^{-2}.

The $AE_{(300\text{-}1350nm)}$ obtained for various mixtures were calculated using the average UV-Vis-IR spectra for the various components and Equations 1-3 and are given in SI Table S2. The selected calculated combination whilst minimising the amount of P-B (the least stable nanofluid in the mixture) was 50% P-A, 20% P-B and 30% P-C, that equates to 0.247 mM final silver concentration in the mixture. This gave a value of $AE_{(300\text{-}1350nm)}$ of 82.52 % which was slightly lower than the optimum mixture without minimizing P-B of 83.14 % (Table S2). Three different batches denoted M-1, M-2 and M-3 were produced using P-A1, P-B1 and P-C1 for M-1, P-A2, P-B2 and P-C2 for M-2 and P-A3, P-B3 and P-C3 for M-3 (where the suffix 1 refers to batch 1, 2 to batch 2 and 3 to batch 3: see Section 2.2). The UV-Vis-IR spectra for the three M batches were then recorded along with transition electron microscopy (TEM) imaging.

2.3 Nanofluids performance under simulated sunlight (SSL)

The set-up of the sunlight simulating system is schematically shown in Figure 1Figure 1. A stabilised power supply (160H x 210L x 200W mm) connected to a xenon light source (output 50 W, collimated spot 30-63 mm diameter, 300-500 nm range), both supplied by Perfect Light Ltd in China, was used to simulate sunlight (model CHF-XM-500W with a PLS SXE300 lamp). Cooling was provided by both a metal fan and radially. The lamp output variation was ± 6 %. A constant setting was used giving a light intensity of 1191 ± 40 Wm^{-2} (measured using a ReRA system calibrated PV cell see SI Table S3).

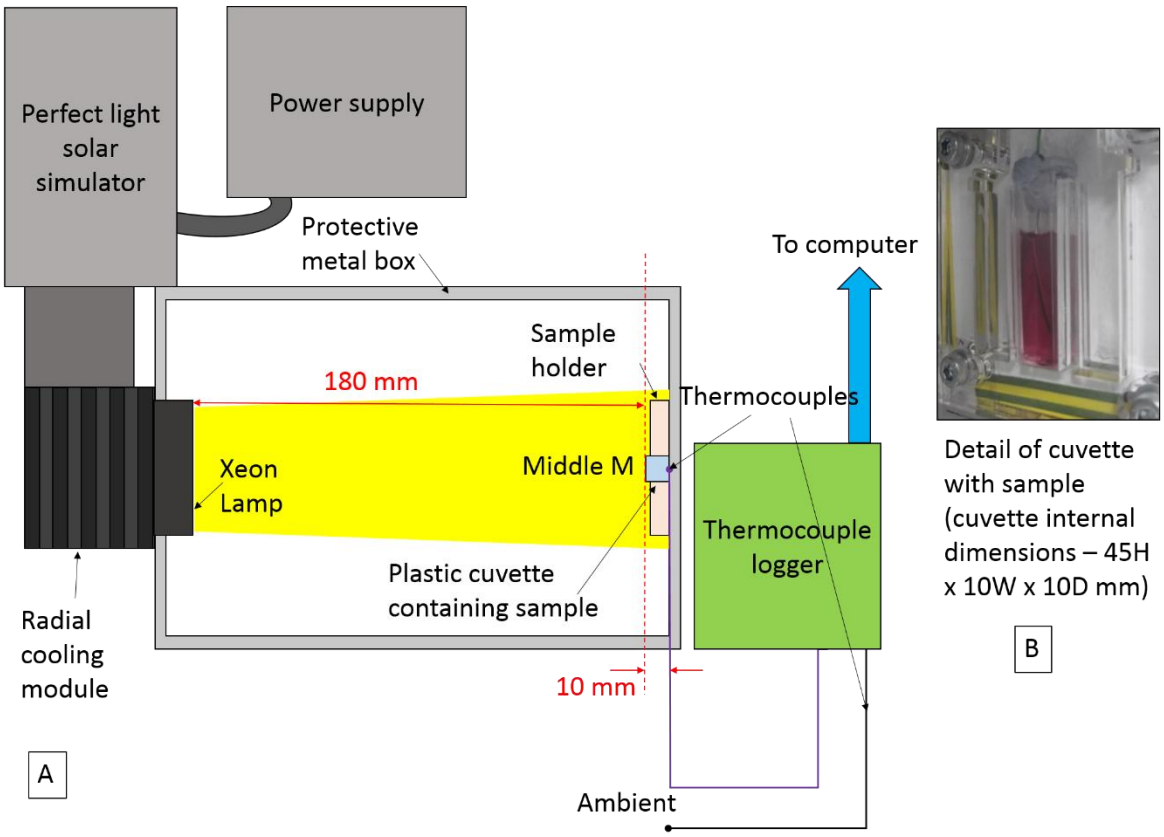

Figure 1 A – Schematic of solar simulator set-up and B – Photograph of sample in cuvette holder with thermocouple

To cover the lamp and provide consistent sample placement (180 mm from lamp to front face of sample) a modified steel metal box was used (300L x 250H x 150D mm, Schneider Electric, Farnell). A sample holder was designed and laser cut from a Perspex sheet. It was bolted to the steel box using 10 mm bolts (not shown) so that the centre of the sample holder was in the centre of the light beam. The temperature of the sample was monitored in real-time using an RS PRO type K thermocouple (diameter 0.6 mm, temperature ranging from –50 to +250 °C) with a welded grounded junction conforming to IEC 60584 standard. Care was taken to ensure the starting temperature of the sample was as consistent as possible at 25 °C ± 1.5 °C. The thermocouple was placed 10 mm from the front face of the sample (see Figure 1A and photograph Figure 1B). The thermocouple was connected to a PC via a National Instruments NI9211 thermocouple data logger with LabVIEW software.

With three batches of P-A, P-B and P-C, and one mixture M prepared the performance under SSL was characterised. Samples P-A and M were measured as prepared, while 1 mL P-B was diluted to

3 mL total volume with water, and 0.6 mL P-C was diluted to 3 mL total volume. The resulting nanofluids were examined before and after SSL exposure using UV-Vis-IR spectroscopy and TEM.

For measurements, a solvent resistant disposable cuvette (Figure 1B) containing 3 mL of sample and the thermocouple was sealed using blue tack and parafilm to prevent evaporation and placed in the sample holder. Samples were exposed to SSL for a period of 10 minutes and then cooled. The measurement was repeated two more times. The UV-Vis-IR spectrum of the sample was then recorded as detailed in Section 2.4. The change in temperature (ΔT) was obtained, as well as the slope of the graph ΔT/Δt in the linear range of the time period (t = 91 - 211 seconds). For a diluted nanofluid, the heat capacity and the mass of nanofluid can be approximated by the heat capacity and mass of the base-fluid. The solar absorption performance in terms of photo-thermal conversion efficiency (PE_{Total}) is determined by Equation 4 (Jin et al., 2016):

$$PE_{Total} = \frac{M_w C_w \Delta T}{A_s I_s \Delta t}$$

Equation 4

where PE_{Total} (%) is the increase in internal energy to total incident solar radiation ratio. The mass of base-fluid is M_w (kg); the base-fluid heat capacity is C_w ($Jkg^{-1}\ K^{-1}$); the temperature change is ΔT (K); the exposed surface area is A_s (m^2), the incident radiative intensity is I_s (Wm^{-2}); and the change in time is Δt (s). The values employed for A_s, M_w, C_w and I_s are shown in Table 1. For the dilute nanofluid the values used for heat capacity and mass were taken as approximately the same as the base-fluid (Jin et al., 2016) – hence the values for the base-fluid for these have been shown. The value for C_w was taken as the average value between 20 and 40 °C for water from (Engineering Toolbox, 2004) (See SI Table S4). The surface area exposed was measured with a ruler and the mass of the base fluid calculated from the volume employed (measured with a micro pippette) using a density of 1000 kgm^{-3}.

Table 1 Values used for the constants in Equation 4. The same values were used for the base-fluid and the nanofluids.

Parameter	Symbol	Unit	Value used
Incident radiative intensity (SI Table S3)	I_s	Wm^{-2}	1191
Surface area exposed	A_s	m^2	0.0003

Heat capacity (Engineering Toolbox, 2004)	C_w	$Jkg^{-1}K^{-1}$	4182
Mass of base fluid	M_w	kg	0.003

The spectra obtained from the Xenon lamp was measured using an Avantes AvaSpec-ULS2048 portable spectroscope (wavelength range: 330 - 1100 nm) and AvaSoft 8 software. The AE for the solar simulator lamp ($AE_{Lamp\ (330\text{-}1100\ nm)}$) was calculated utilising this spectra and the UV-Vis-IR spectra obtained for the mixture and components according to Equation 5 where $\sum_{\lambda=330}^{\lambda=1100} P_{i\ lamp(\lambda)}$ is the incident power intensity of the lamp over the wavelength range 330 – 1100 nm. As the spectroscope does not give a power intensity, the spectra obtained for the lamp was normalised, and then the area under the spectral curve was used to approximate $\sum_{\lambda=330}^{\lambda=1100} P_{i\ lamp(\lambda)}$.

$$AE_{Lamp\ (330-1100\ nm)} = \frac{\sum_{\lambda=330}^{\lambda=1100} P_{Ab(\lambda)}}{\sum_{\lambda=330}^{\lambda=1100} P_{i\ lamp(\lambda)}} \times 100$$

Equation 5

The calculated $AE_{Lamp\ (330\text{-}1100\ nm)}$ was then compared to the value of PE_{Total} obtained from Equation 4.

2.4 Characterisation of nanofluids and nanoparticles

UV-Vis-IR spectroscopy analysis was performed with a spectrophotometer (Perkin Elmer Lambda 750S) over a wavelength range of 300 - 1300 nm at a scan rate of 204.74 nm min^{-1}, and a scan step of 1 nm s^{-1}. Disposable cuvettes (light path length, 10 mm) were used, with base-fluid and cuvette correction being employed. If a quartz rather than plastic cuvette had been employed there would be some differences especially in the IR region. However, for consistency and ease of experimentation plastic cuvettes were used for this study. A full comparison between different optical materials for the cuvettes is beyond the scope of this work but will be assessed in future studies.

A Hitachi HT7700 100 kV was used for Transmission electron microscope (TEM) analysis. Samples were prepared on Formvar and carbon coated 200 mesh Cu/Pd grids by drop-casting the colloid

solution and allowing the base-fluid to evaporate. Digimizer software was used to further analyse the samples using the TEM image scale bar to calibrate the line length. Manual size measurement of individual nanoparticles was employed, dividing the particles into different shape categories. For triangular particles, the length of the longest side of the triangle was measured and for discs or spheres, the diameter. Using more than one image of each sample provided a statistically adequate number of measurements.

2.5 Uncertainty analysis

The method employed by (Bell, 2001) and used previously (Kimpton et al., 2020)was used to determine the measurement uncertainty. The calibration / resolution equipment uncertainties (type B) were estimated for the three measurement types (SSL, TEM and UV-Vis-IR). These were added to the sample variation (type A) uncertainties providing a combined relative uncertainty. A final expanded uncertainty was then obtained by using a coverage factor of 2 (about 95% confidence).

The constant M_wC_w/A_sI_s (Equation 4) uncertainties for the SSL tests (type B) resulted in an expanded uncertainty of 8.18 % (SI Table S4). When combined with the sample variation (SI Table S5) the uncertainty range was between 8.24 and 10.37 %. Type B uncertainties from the UV-Vis-IR measurements and subsequent AE calculations were much lower being < 1% (See SI Table S6), giving a combined total when the type A sample variations were added (SI Table S7) of between 1.18 and 6.69%. The type B uncertainties arising from the TEM measurements were <3%. Even with the use of multiple images to increase the number of measurements the particle size variation gave rise to larger type A variation and hence expanded uncertainty (shown for P-A triangles before SSL in SI Table S8) – giving expanded uncertainties of between 6.03 and 9.10% for the TEM measurements. This value does not account for any errors associated with choosing the particle shape manually from the TEM image.

3 RESULTS AND DISCUSSION

3.1 UV-Vis-IR characterisation

The UV-Vis-IR characterisation of the three nanofluids prior to mixing are shown in Figure 2. The mean values of the three repeats are shown both initially and after storage in the dark at 4°C for 4 weeks (individual results are reported in SI, Figures S1, S2 and S3, Tables S9, S10 and S11). As can be seen, three nanofluids exhibited distinguishing spectra with clearly three different positions of corresponding maximum absorption peak (λ_{max}). For nanofluid P-A, λ_{max} was 929 ± 31.8 nm initially. After 4 weeks of storage the mean value remained approximately the same. The peak height (H_{peak}) was 1.577 ± 0.03 au initially, with a slight drop to 1.538 ± 0.02 au after 4 weeks. For nanofluid P-B, λ_{max} was initially 667 ± 7.9 nm with an H_{peak} of 1.342 ± 0.03 au. After 4 weeks of storage in the dark, λ_{max} red shifted to a value of 709 ± 6.1 nm while H_{peak} stayed approximately the same. Finally, for nanofluid P-C, λ_{max} was 468 ± 24.8 nm initially, and 472 ± 23.4 nm after 4 weeks whereas H_{peak} was 0.708 ± 0.06 au initially, and 0.709 ± 0.03 au without noticeable change after storage. The only significant change (see SI for significance testing) was the noticeable red shift in λ_{max} for P-B. Because of this reduction in stability observed for P-B the amount of P-B in the mixture M was kept to a minimum (see Section 2.2). The shift in λ_{max} could be due to morphological changes in the AgNPs with time (a sharpening of the corners of the rounded prisms and or an increase in size could lead to a red shift being observed) and represents additional information, which is obtained from undertaking experimental rather than numerical studies. Nevertheless, the measurements before and after 4 weeks storage showed all three colloidal nanofluids to be relatively stable, with a higher level of stability than that previously observed for colloidal silver (Haber and Sokolov, 2017).

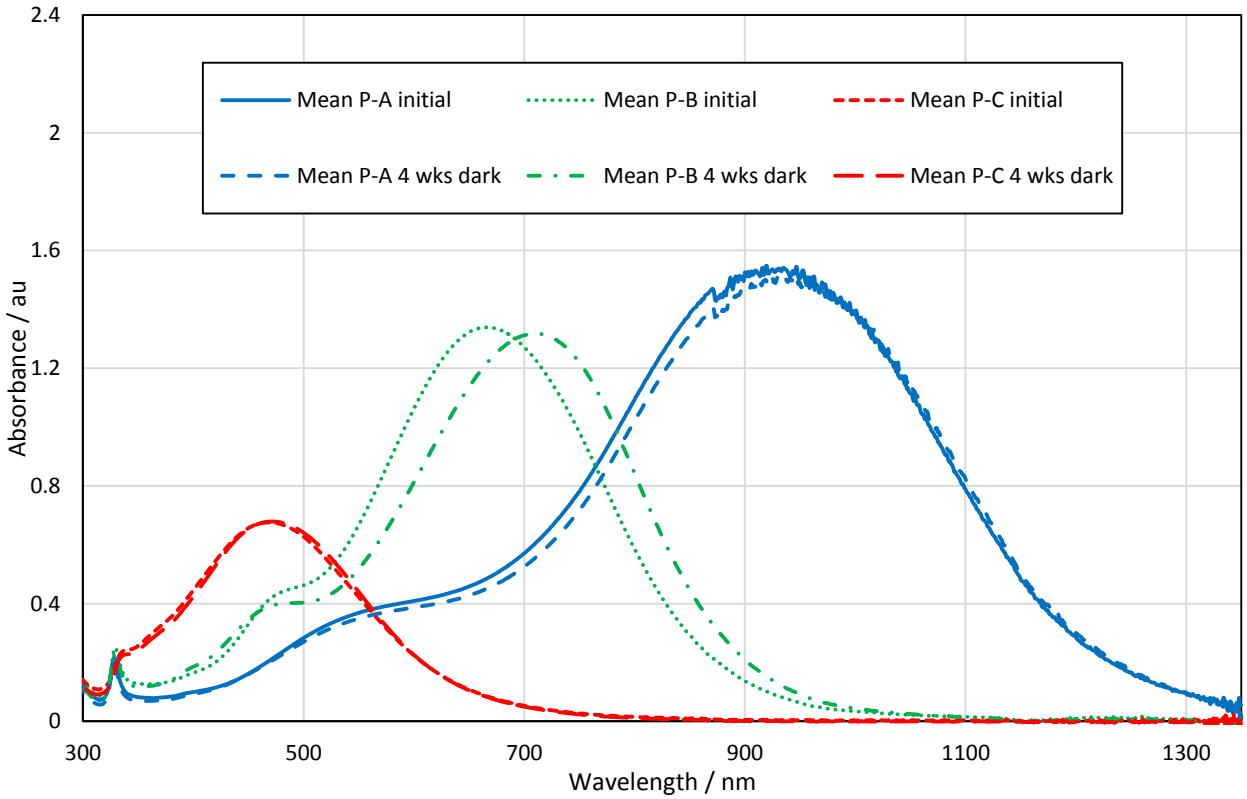

Figure 2 UV-Vis-IR spectra for P-A, P-B and P-C initially, and after 4 weeks storage in the dark at 4°C (4 wks dark). Mean values shown. Note that P-B was diluted 1 mL in 3 mL, and P-C was diluted 0.6 mL in 3 mL. All measurements undertaken with a 10 mm path length cuvette.

Figure 3 shows the results of calculating the absorbance for the mixture based on the spectra obtained for the P-A, P-B and P-C components along with the actual spectra obtained when the mixture was measured (both initially and after storage in the dark at 4°C). Again, the mean values are shown (for the individual values please see SI Figures S4 and S5 and Table S12). For the actual mixture there was a red shift of about 100 nm in the secondary λ_{max} corresponding to the P-B component compared to the calculated value. The primary λ_{max} due to component P-C in contrast was similar for both the calculated and measured spectra. The cause of the red shift in the secondary λ_{max} is unknown but may be related to the smaller but similar red shift observed on storage for P-B and is additional information which is obtained by carrying out experimental studies. This shift was consistent across the three M samples (see Figures S4 and S5). The mixture was, however, stable with storage for 4 weeks in the dark, with no shift in the primary or secondary λ_{max} being observed (see Figure S5 and Table S13).

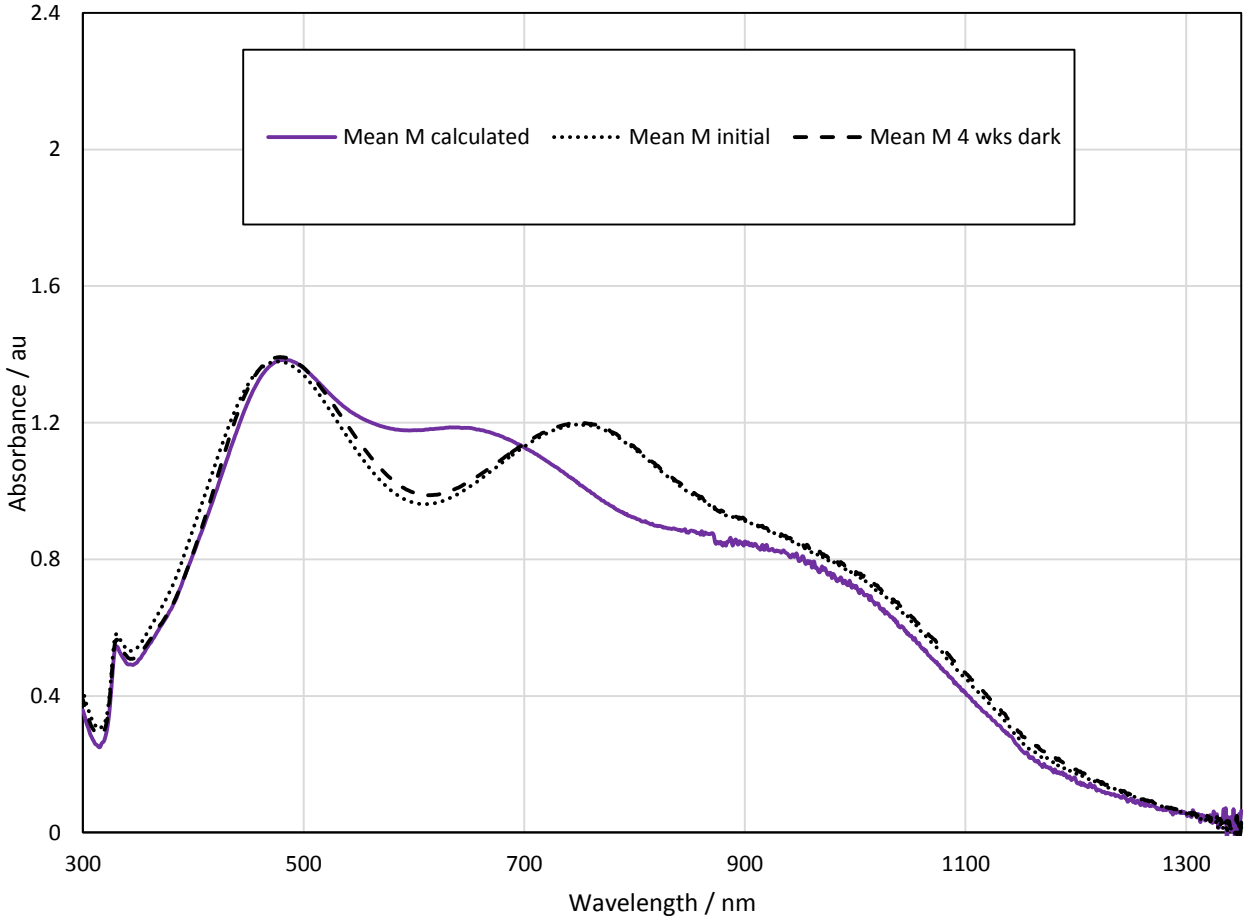

Figure 3 UV-Vis-IR spectra for the mixture M, calculated from the component spectra and as measured initially and after 4 weeks storage in the dark at 4°C. Mean values shown. All measurements undertaken with a 10 mm path length cuvette.

3.2 TEM analysis of as produced nanofluids

TEM analysis of samples P-A, P-B, P-C and the mixture M (Figure 4 and SI Table S14) showed that P-A consisted primarily of triangles with sharp corners with a mean size of 52.2 ± 17.6 nm and a thickness of 5.9 ± 2.6 nm. P-B consisted mainly of smaller triangles (mean size 27.5 ± 7.6 nm) and rounded cornered triangles (mean size 23.7 ± 6.7 nm) which were slightly thinner (mean thickness 4.7 ± 1.3 nm). P-C consisted mainly of small (< 10 nm) particles and slightly larger disc-like particles (diameter 15.9 ± 4.2 nm, thickness 5.0 ± 1.1 nm). As expected the mixture M (Figure 4 D) contained all types of particles, with larger sharp cornered triangles, smaller rounded corner triangles, disc-like particles and small (< 10 nm) particles being present.

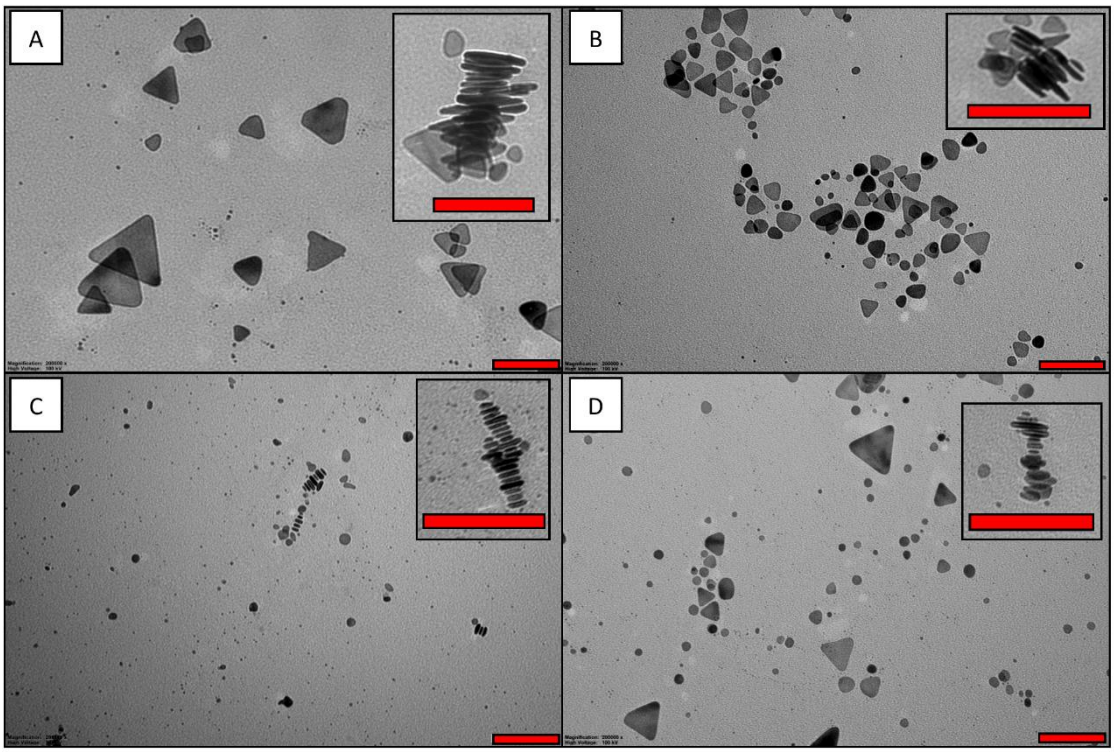

Figure 4 TEM images of A) P-A, B) P-B, C) P-C and D) M before solar simulator testing. The magnified inserts show the edges and thicknesses of the nanoparticles. All scale bars including the ones in the inserts = 100 nm

3.3 Calculating the performance of nanofluids from UV-Vis-IR spectra based absorption

In this work the measured absorption was used directly to calculate the power absorbed rather than the extinction coefficient used by others (Jeon et al., 2014). This approach, on one hand, overcame the difficulty of estimating the extinction coefficient for non-spherical metallic particles (while only spherical and nanorods have been estimated previously) (Gorji and Ranjbar, 2017; Jeon et al., 2014). It was valid as absorption was representative of extinction coefficient for nanofluids of low particle loading without aggregation (i.e. with insignificant scattering effect)(Gorji and Ranjbar, 2015, 2017). On the other hand, it was difficult to compare the results obtained in this work with those reported through extinction coefficient estimation.

According to Equation 2, from the absorption spectra, the power absorbed at different wavelengths relative to the incident solar power intensity can be calculated. The results for three component nanofluids, i.e. P-A, P-B and P-C, and the mixture M, are shown graphically in Figure 5. The calculated value for M and the power intensity not absorbed by the mixture are also shown. Here it can be seen that M absorbs a larger proportion of the power than each of the three

components over a broader wavelength range up to about 1100 nm. In the 1100 – 1350 nm range the performance of the mixture reduced, with only a small proportion of the incident solar power being absorbed. The reasons for this are two-fold, firstly the amount of P-A, which is only a weak absorber in this region, in M is only 50% this reduces the power absorbed in this region due to the AgNPs. Secondly, as base-line correction for the base-fluid was used to undertake the UV-Vis-IR measurements any absorption due to the base-fluid water in this region would not be accounted for. As water absorbs more strongly in this region (Mallah et al., 2018), this leads to an under estimation of the power absorbed by the combination of the AgNPs and the base-fluid (i.e. the nanofluid) above 1100 nm.

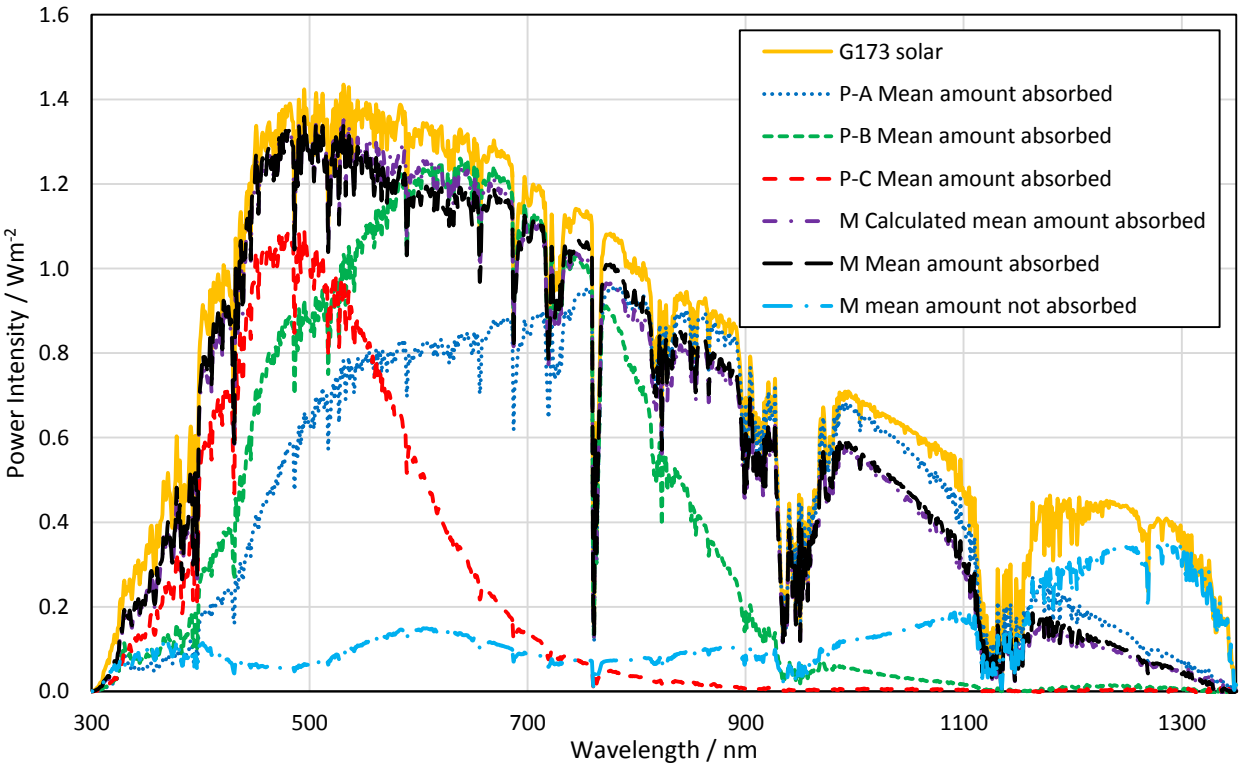

Figure 5 Amount of the G173 solar reference spectral power absorbed at different wavelengths by P-A, P-B, P-C and M. Mean results shown (Complete results given in SI Figures S6 – S10). The amount of the solar spectrum not absorbed by the mixture M is also shown. Calculation uses the same dilution for P-B and P-C as used for the UV-Vis-IR measurements

A comparison between the spectral response of the lamp used for the SSL testing and the G173 Solar spectrum is given in Figure 6. Here it can be seen that there are some differences between the two spectra especially in the 800 – 1100 nm range. Because of these differences $AE_{Lamp\ (330\text{-}1100\ nm)}$ was calculated (see Equation 5) from the UV-Vis-IR spectra to allow comparison with the

results obtained for PE_{Total} obtained from direct measurement of the temperature rise in the solar simulator.

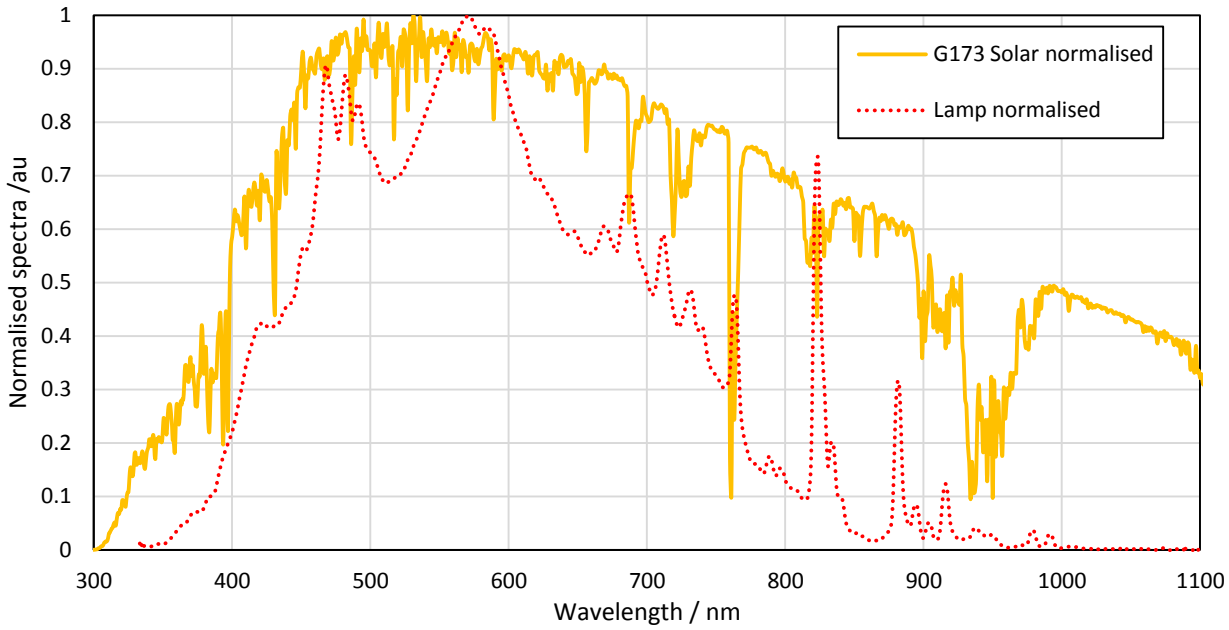

Figure 6 Spectral response of the SSL lamp compared to the G173 solar reference spectra. Both spectra have been normalised for comparison

Using Equation 5, $AE_{Lamp\ (330\text{-}1100\ nm)}$ was calculated from the UV-Vis-IR spectral data for the mixture M and the three component nanofluids. The results are shown in Table 2. Analysis of variance (ANOVA – see SI for details) was undertaken on the data to determine if $AE_{Lamp\ (330\text{-}1100\ nm)}$ for the mixture M was greater than the three nanofluids used for the mixture and to estimate the likely range of the value at a 95% confidence interval. The $AE_{Lamp\ (330\text{-}1100\ nm)}$ of the mixture was greater than 90% showing the potential of this blended nanofluid for solar applications.

Table 2 Results of calculating $AE_{Lamp\ (330\text{-}1100\ nm)}$ *from the UV-Vis-IR data.*

Nanofluid type	**n***	**Grouping**	**Mean $AE_{Lamp\ (330\text{-}1100\ nm)}$ / %**	**Standard deviation (StDev) / %**	**95% confidence interval (CI) for the mean**
P-A	9	B	57.81	1.78	56.01 – 59.62
P-B	9	C	73.97	2.02	72.17 – 75.78
P-C	9	D	46.29	4.61	44.49 – 48.10
M	12	A	92.75	1.37	91.18 – 94.31

** n = number of measurements. The initial, after 4 weeks storage and after exposure to SSL for 30 minutes has been used giving n = 9. In addition for M the calculated spectral data has been included (hence for M, n = 12). Means that do not share the same letter are significantly different (see analysis of variance section in SI)*

Using the actual reference solar spectrum over the extended wavelength range of 300-1350 nm (Equation 3) gives a better indication of the potential performance of the broadband mixture M in sunlight. It should be noted that, although the AE value of mixture M appeared to be greater than 80% (see SI Table S15), it was based on the assumption that all the energy from the solar spectrum outside of the 300 -1350 nm range was absorbed. Therefore, the actual performance of the broadband absorber is likely to be slightly below 80%. Nevertheless, this performance is still impressive for a very dilute nanofluid, showing the benefit of both utilising a plasmonic nanofluid and tailoring the response of that nanofluid by varying the nanoparticle geometry in the fluid to closely match the solar spectra. It should also be noted that all these calculations were undertaken using a light path length of 10 mm. If the path length or the concentration of M was increased, the performance of this blended nanofluid could be further improved. On the other hand, increasing the concentration may, have a detrimental effect on the colloidal stability. Conversely, reducing the nanofluid concentration would potentially improve colloidal stability, but a greater depth of nanofluid would be needed to give the same performance. This would require further investigation.

3.4 Thermal performance of nanofluids under SSL

The thermal performance of nanofluids subject to SSL exposure was measured by monitoring the temperature rise over a period of 10 minutes. The measured temperature profiles on exposure to SSL for the three component nanofluids and the blended broadband mixture are shown in Figure 7, along with the profile for water. The initial temperature recorded at the start of each experiment was 25.7 °C (StDev 0.6 °C N = 39). The nanofluids all exhibited an initial linear temperature rise with time, followed by a decrease in the rate of temperature rising. The trend indicated that, if the time of the experiments was extended, the temperature profile would level out as the stagnation temperature was reached (i.e. the rate of heat loss became equal to the rate of heat gain).

As shown in Equation 4, with a given absorber and irradiation source, the thermal performance is determined by $\Delta T/\Delta t$, the initial slope of the linear temperature rise. Therefore, for these experiments it was not deemed necessary to continue the experiment beyond the linear rise stage, or until the saturation temperature was reached. In addition, if care had not been taken to maintain a consistent starting temperature of the nanofluid, there may have been some variation in the length of the linear portion of the graph, requiring that the slope was calculated over a smaller Δt. However, it should not greatly affect the value of PE obtained (especially when the experimental uncertainties of 8.24 – 10.37 % are considered), unless a significantly higher starting temperature at or near the stagnation temperature was used leading to no linear region on the graph. Further investigation of the effect of starting temperature would be needed to confirm this.

All of the nanofluids exhibited a significantly greater ΔT than water with the M nanofluids showing the largest increase, followed by P-B, P-A and then P-C, in line with the order observed for absorption efficiency $AE_{Lamp\ (330\text{-}1100\ nm)}$. By using the $\Delta T/\Delta t$ values (Figure 7), PE_{Total} values for all four samples were obtained. The results summarised in Table 3, show good agreement with the values obtained for $AE_{Lamp\ (330\text{-}1100\ nm)}$ (Table 2). This is especially valid when the measurement uncertainties of 8.24 – 10.37 % (Section 2.5) are taken into consideration.

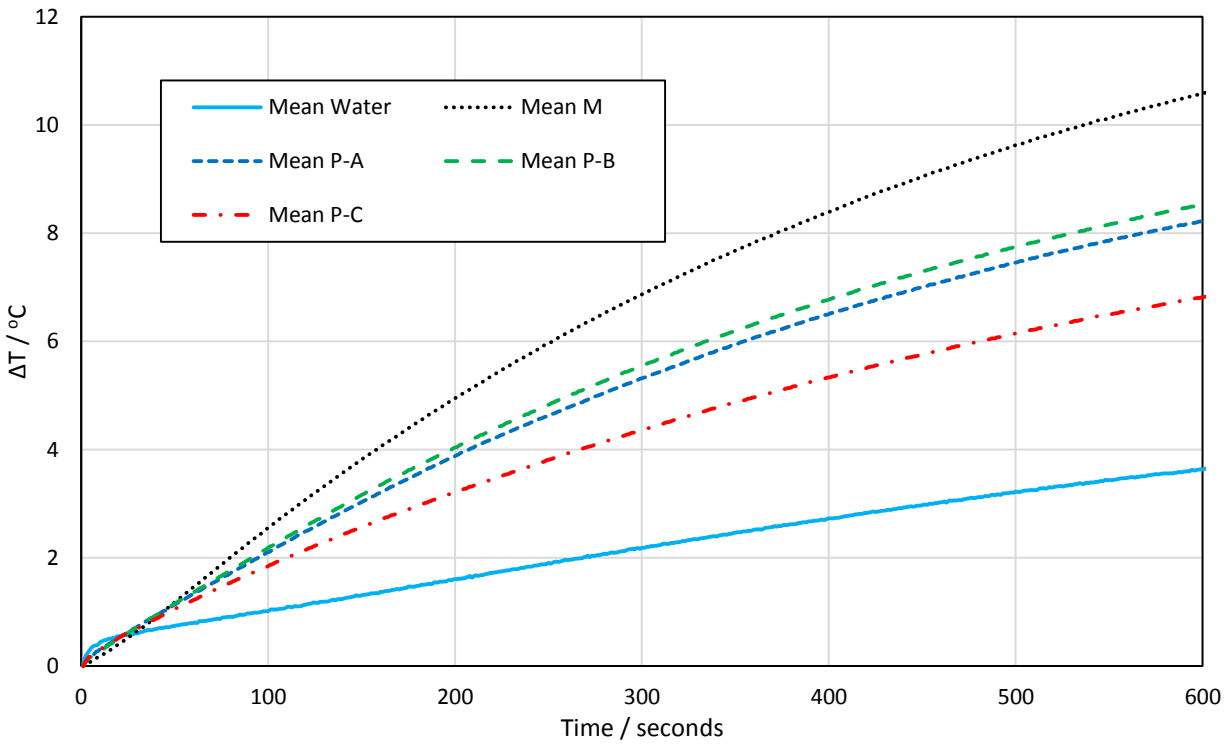

Figure 7 Change in temperature with time of exposure to SSL for the mixture M and components P-A, P-B and P-C. The mean results from 9 measurements per sample type are shown except for water where n = 3

Table 3 Calculated values of PE_{Total} obtained from SSL testing. ANOVA testing (See SI) was undertaken to determine the significance of the results and to determine the possible range of the mean values (at 95% CI). Samples that do not share the same letter are significantly different

Nanofluid type	n*	Grouping	Mean PE_{Total} from SSL / %	StDev / %	95% CI for the mean
Water	3	D	20.51	1.17	14.61 – 26.34
M	9	A	83.77	2.29	80.40 – 87.14
P-A	9	B	62.46	4.49	59.09 – 65.83
P-B	9	B	65.05	7.58	61.68 – 68.42
P-C	9	C	47.68	4.68	44.31 – 51.05

** Number of repeated measurements.*

As discussed above, there is no direct comparison between the results obtained here and those with a blended mixture of gold by Jeon et al (Jeon et al., 2016) who used extinction coefficients for calculation under different conditions, such as using a computer model to calculate efficiency under flow conditions based on static experimental data. Interestingly, their blended gold absorber appeared to give a comparable level of maximum efficiency at about 80-85 %, which is similar to the results obtained in this study (83.77%).

In addition, the silver nanofluid with the two absorption peaks produced by Walshe et al (essentially a mixture with an absorbance covering the range 300 -750 nm) also gave a PE value of about 90%, similar to this study. These results were also obtained from static testing while using different sample geometry and testing protocol. The numerical study by Mallah et al (Mallah et al., 2018) produced better results for efficiency than this study at a lower concentration but with a longer path length employed (up to 98 % for a 10 cm path length). The absorption obtained in the near IR range was better for the nanofluid they proposed containing silver nanorods. To give a true comparison to this work a five component nanofluid with the same concentrations, nanoparticle types and ratio of components would need to be synthesised and tested using the same geometry as they proposed. In fact in their conclusions they acknowledge the importance of conducting experimental studies on these blended nanofluids.

3.5 Characterisation of nanofluids after SSL

To assess the stability of nanofluids subject to light exposure, they were examined with both UV-Vis-IR spectroscopy and TEM following exposure to SSL for 30 minutes for the mixture and three component nanofluids. It was found that there were some changes in the spectra (Figure 8). λ_{max} for nanofluid P-A had blue shifted by approximately 50 nm with a small but significant drop of 5% in H_{peak} (SI Table S16). Nanofluid P-B exhibited a greater blue shift of about 90 nm in λ_{max} with an increase of about 9% in H_{peak}. Nanofluid P-C showed a slight red shift in λ_{max} (see Table S17) but a significant increase of 45 % in H_{peak}. The mixture M also exhibited this significant increase in H_{peak} for the primary peak, mainly due to the contribution of P-C to the spectra. The shape of the spectra for M also changed due to the blue shift in λ_{max} of both P-A and P-B.

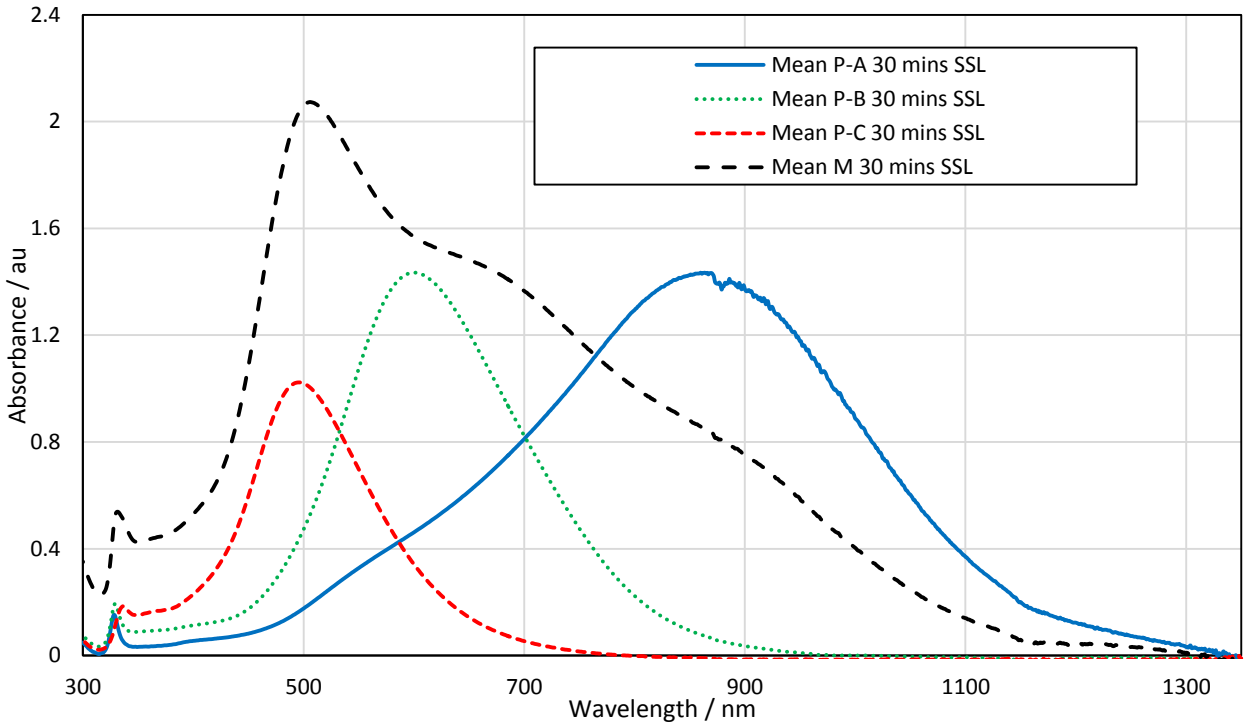

Figure 8 UV-Vis-IR spectra for M, P-A, P-B and P-C after 30 minutes exposure to SSL. Mean values shown. Note that P-B was diluted 1 mL in 3 mL, P-C was diluted 0.6 mL in 3 mL. All measurements undertaken with a 10 mm path length cuvette.

TEM images of P-A, P-B, P-C and the mixture M after SSL are shown in Figure 9. A more detailed size analysis is presented in SI Table S18. It was found that the triangles in sample P-A became more rounded, and in P-B the rounded triangles were even further rounded and mixed with disc-

shaped. To confirm the hypothesis that the disc-shaped particles were derived from the triangles, the percentage of each type of particles was estimated, and the results are shown in Figure 10. As can be seen, the number of rounded corner triangles increased for P-A and the number of other shaped particles (discs and hexagons) increased for P-B. The average size and thicknesses of the particles appeared to be unchanged (Table S18). Hence, the predominate mechanism for this change was believed to be the rounding of the sharp corners of the triangles in P-A, causing a blue shift in the UV-Vis-IR spectra, while a further rounding of the already rounded corner triangles in P-B to more disc-shaped particles. This losing of the sharp corners of silver nanoprisms has been observed previously by others, largely associated with the mechanical and physiochemical properties of the sharp tips (Roh et al., 2012; Tang et al., 2013; Taylor et al., 2018).

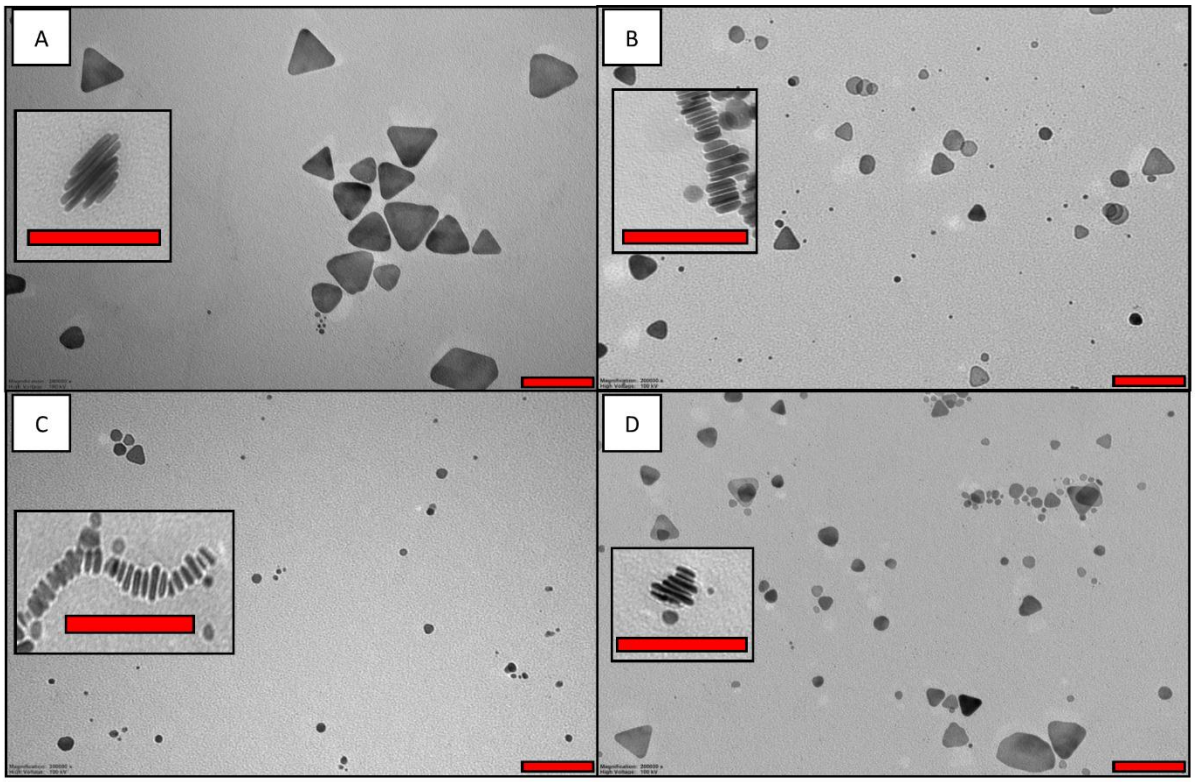

Figure 9 TEM images of A) P-A, B) P-B, C) P-C and D) M after solar simulator testing. The magnified inserts show the edges of the nanoparticles. All scale bars All scale bars including the ones in the inserts = 100 nm

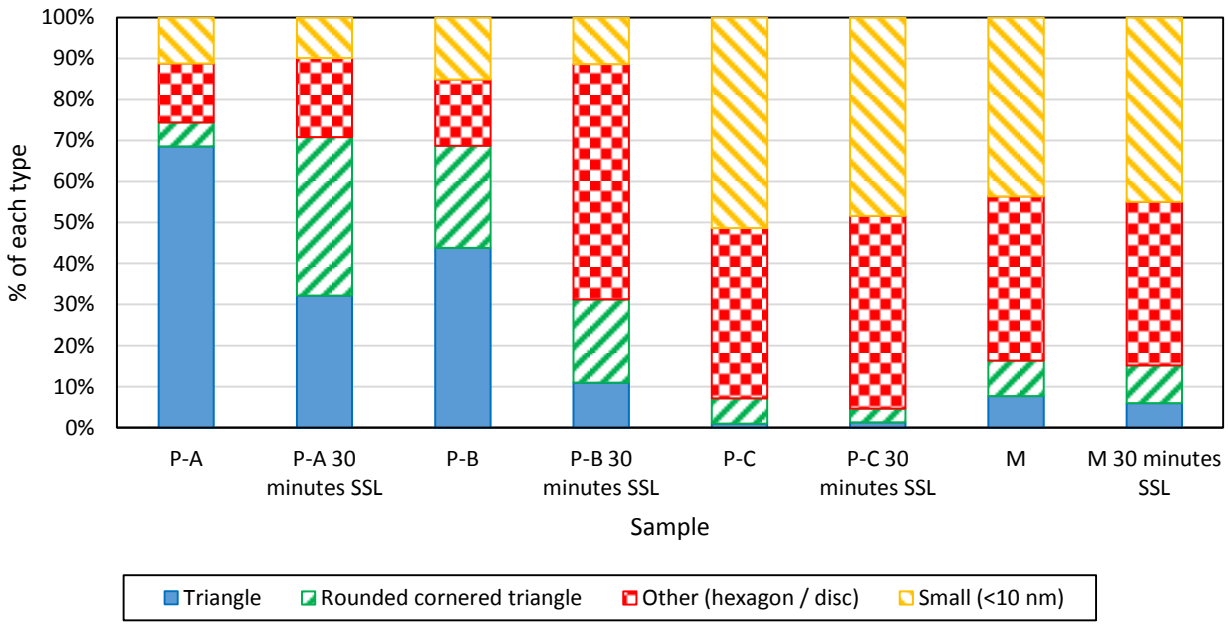

Figure 10 Percentage of each type of particle before and after SSL exposure estimated from TEM micrographs for P-A, P-B, P-C and M

There are a number of potential ways to reduce the instability of silver nanofluids towards photo-induced shape change. The modification of the pH of the nanofluid has been proposed with the addition of OH^- ions (Roh et al., 2012). Coating the silver nanoparticle with e.g. SiO_2 has been explored (Hjerrild et al., 2018; Taylor et al., 2018). This is also an ongoing active research topic in our laboratories (Kimpton et al., 2020).

4 CONCLUSIONS AND FURTHER WORK

For the first time a silver nanofluid-based broadband absorber consisting of three different nanoparticles was produced, and its potential for enhancing solar thermal capture was demonstrated experimentally towards application in direct absorption solar collectors (DASCs). A batch process was used to consistently synthesise three different silver nanofluids with absorption peaks in the ranges 880 -980 nm, 650-750 nm and 450 -520 nm, respectively, just by variation in the amount and timing of the chemical additions. The potential absorption efficiency (AE) was calculated from UV-Vis-IR spectra, and the computed value was compared to the value obtained by measuring real time temperature rise of the nanofluids in a solar simulator.

Comparable results were obtained through the two approaches, i.e. by estimating an average absorption efficiency $AE_{Lamp\ (330\text{-}1100\ nm)}$ with the UV-Vis-IR method (92.75 ± 1.37%), and an average photo-thermal conversion efficiency PE_{Total} of 83.77 ± 2.29 % using the solar simulator method. The similarity of the results obtained enables calculations based on UV-Vis-IR measurements to be used with confidence for the rapid identification and screening of nanofluids for their potential in DASC applications.

Although the nanofluids and mixture were shown to have good colloidal stability after storage in the dark for 4 weeks at 4°C, the story was not the same following light exposure. Subjected to simulated sunlight exposure, the nanoparticles showed a change in absorption spectra and morphology even after only 30 minutes exposure. This is additional information directly confirmed by TEM imaging, but not by the initial UV-Vis-IR spectroscopy. This clearly demonstrates the value of utilising complementary techniques for the assessment of a nanofluids suitability for DASC applications. Although the results presented here are limited to the specific nanofluids tested, they provide useful guidelines for other researchers in determining suitable assessment techniques for their nanofluids.

Due to the instability of the silver nanofluids shown here, a suitable coating or stabilisation strategy would be required for further development of this broadband absorber for solar energy capture applications. Nonetheless, compared to the timeframe of conventional surface-based solar collectors (i.e. 20 years), it will still be challenging to make a silver-based nanofluid for long-term running in the harsh environmental conditions experienced. This lack of long-term stability has been muted as one of the reasons hindering DASCs commercialisation (Sharaf et al., 2019).

Further work will firstly focus on the effect of temperature alone on the broadband absorber stability as it is important to determine if the instability is due to the solar radiation or a combination of solar radiation and heat. The focus will then shift to measuring the broadband absorber under flow conditions to get a better understanding of potential performance and stability to mechanical damage. After this, methods of stabilising the silver morphology will be investigated in the hope that the broadband absorber developed here could be made more suitable for solar energy applications.

5 ACKNOWLEDGEMENTS

The authors acknowledge the support of the EPSRC-funded CDT in Energy Storage and Its Applications and the Faculty of Engineering and Physical Sciences both at the University of Southampton. They would especially like to thank Thomas Mercier for his assistance with the lamp intensity measurements using the ReRA system calibrated PV cell, and Associate Professor Dmitry Bavykin and Professor Andrew Cruden for their valuable discussions.

6 REFERENCES

Abdelrazik, A.S., Al-Sulaiman, F.A., Saidur, R., 2019. Optical behavior of a water/silver nanofluid and their influence on the performance of a photovoltaic-thermal collector. Solar Energy Materials and Solar Cells, 201, 110054, https://doi.org/10.1016/j.solmat.2019.110054.

Aherne, D., Ledwith, D.M., Gara, M., Kelly, J.M., 2008. Optical Properties and Growth Aspects of Silver Nanoprisms Produced by a Highly Reproducible and Rapid Synthesis at Room Temperature. Advanced Functional Materials, 18(14), 2005-2016, https://doi.org/10.1002/adfm.200800233.

Ahmad, S.H.A., Saidur, R., Mahbubul, I.M., Al-Sulaiman, F.A., 2017. Optical properties of various nanofluids used in solar collector: A review. Renewable and Sustainable Energy Reviews, 73, 1014-1030, https://doi.org/10.1016/j.rser.2017.01.173.

ASTM, 2012. Reference Solar Spectral Irradiance: ASTM G-173. https://rredc.nrel.gov/solar//spectra/am1.5/ASTMG173/ASTMG173.html. (Accessed 01 July 2019.

Bandarra Filho, E.P., Mendoza, O.S.H., Beicker, C.L.L., Menezes, A., Wen, D., 2014. Experimental investigation of a silver nanoparticle-based direct absorption solar thermal system. Energy Conversion and Management, 84, 261-267, https://doi.org/10.1016/j.enconman.2014.04.009.

Bastys, V., Pastoriza-Santos, I., Rodríguez-González, B., Vaisnoras, R., Liz-Marzán, L.M., 2006. Formation of Silver Nanoprisms with Surface Plasmons at Communication Wavelengths. Advanced Functional Materials, 16(6), 766-773, https://doi.org/10.1002/adfm.200500667.

Bell, S., 2001. A Beginner's Guide to Uncertainty of Measurement. NPL, UK TW11 0LW, https://www.dit.ie/media/physics/documents/GPG11.pdf. (Accessed 20 November 2019).

Carboni, M., Capretto, L., Carugo, D., Stulz, E., Zhang, X., 2013. Microfluidics-based continuous flow formation of triangular silver nanoprisms with tuneable surface plasmon resonance. Journal of Materials Chemistry C, 1(45), 7540, https://doi.org/10.1039/c3tc31335b.

Carboni, M., Carravetta, M., Zhang, X.L., Stulz, E., 2016. Efficient NIR light blockage with matrix embedded silver nanoprism thin films for energy saving window coating. J. Mater. Chem. C, 4(8), 1584-1588, https://doi.org/10.1039/c6tc00026f.

Chen, M., He, Y., Zhu, J., Wen, D., 2016. Investigating the collector efficiency of silver nanofluids based direct absorption solar collectors. Applied Energy, 181, 65-74, https://doi.org/10.1016/j.apenergy.2016.08.054.

Crisostomo, F., Hjerrild, N., Mesgari, S., Li, Q., Taylor, R.A., 2017. A hybrid PV/T collector using spectrally selective absorbing nanofluids. Applied Energy, 193, 1-14, https://doi.org/10.1016/j.apenergy.2017.02.028.

Du, M., Tang, G.H., 2016. Plasmonic nanofluids based on gold nanorods/nanoellipsoids/nanosheets for solar energy harvesting. Solar Energy, 137, 393-400, https://doi.org/10.1016/j.solener.2016.08.029.

Duffie, J.A., Beckman, W.A., 2013. Solar Engineering of Thermal Processes, Fourth Edition. John Wiley & Sons.

Engineering Toolbox, 2004. Water - Specific Heat. https://www.engineeringtoolbox.com/specific-heat-capacity-water-d_660.html. (Accessed 21 January 2020.

Goel, N., Taylor, R.A., Otanicar, T., 2020. A review of nanofluid-based direct absorption solar collectors: Design considerations and experiments with hybrid PV/Thermal and direct steam generation collectors. Renewable Energy, 145, 903-913, https://doi.org/10.1016/j.renene.2019.06.097.

Gorji, T.B., Ranjbar, A.A., 2015. Geometry optimization of a nanofluid-based direct absorption solar collector using response surface methodology. Solar Energy, 122, 314-325, https://doi.org/10.1016/j.solener.2015.09.007.

Gorji, T.B., Ranjbar, A.A., 2016. A numerical and experimental investigation on the performance of a low-flux direct absorption solar collector (DASC) using graphite, magnetite and silver nanofluids. Solar Energy, 135, 493-505, https://doi.org/10.1016/j.solener.2016.06.023.

Gorji, T.B., Ranjbar, A.A., 2017. A review on optical properties and application of nanofluids in direct absorption solar collectors (DASCs). Renewable and Sustainable Energy Reviews, 72, 10-32, https://doi.org/10.1016/j.rser.2017.01.015.

Gupta, H.K., Agrawal, G.D., Mathur, J., 2015. Experimental Evaluation of Using Nanofluid in Direct Absorption Solar Collector, Energy Technology & Ecological Concerns: A Contemporary Approach. 150-154.

Haber, J., Sokolov, K., 2017. Synthesis of Stable Citrate-Capped Silver Nanoprisms. Langmuir, 33(40), 10525-10530, https://doi.org/10.1021/acs.langmuir.7b01362.

Hjerrild, N.E., Scott, J.A., Amal, R., Taylor, R.A., 2018. Exploring the effects of heat and UV exposure on glycerol-based Ag-SiO_2 nanofluids for PV/T applications. Renewable Energy, 120, 266-274, https://doi.org/10.1016/j.renene.2017.12.073.

Iyahraja, S., Rajadurai, J.S., 2015. Study of thermal conductivity enhancement of aqueous suspensions containing silver nanoparticles. AIP Advances, 5(5), 057103, https://doi.org/10.1063/1.4919808.

Jeon, J., Park, S., Lee, B.J., 2014. Optical property of blended plasmonic nanofluid based on gold nanorods. Opt Express, 22 Suppl 4, A1101-1111, https://doi.org/10.1364/OE.22.0A1101.

Jeon, J., Park, S., Lee, B.J., 2016. Analysis on the performance of a flat-plate volumetric solar collector using blended plasmonic nanofluid. Solar Energy, 132, 247-256, https://doi.org/10.1016/j.solener.2016.03.022.

Jin, H., Lin, G., Bai, L., Amjad, M., Bandarra Filho, E.P., Wen, D., 2016. Photothermal conversion efficiency of nanofluids: An experimental and numerical study. Solar Energy, 139, 278-289, https://doi.org/10.1016/j.solener.2016.09.021.

Kazemi-Beydokhti, A., Heris, S.Z., Moghadam, N., Shariati-Niasar, M., Hamidi, A.A., 2014. Experimental Investigation of Parameters Affecting Nanofluid Effective Thermal Conductivity. Chemical Engineering Communications, 201(5), 593-611, https://doi.org/10.1080/00986445.2013.782291.

Khullar, V., Tyagi, H., Hordy, N., Otanicar, T.P., Hewakuruppu, Y., Modi, P., Taylor, R.A., 2014. Harvesting solar thermal energy through nanofluid-based volumetric absorption systems.

International Journal of Heat and Mass Transfer, 77, 377-384, https://doi.org/10.1016/j.ijheatmasstransfer.2014.05.023.

Kimpton, H., Cristaldi, D.A., Stulz, E., Zhang, X., 2020. Thermal performance and physicochemical stability of silver nanoprism-based nanofluids for direct solar absorption. Solar Energy, 199, 366-376, https://doi.org/10.1016/j.solener.2020.02.039.

Ledwith, D.M., Whelan, A.M., Kelly, J.M., 2007. A rapid, straight-forward method for controlling the morphology of stable silver nanoparticles. Journal of Materials Chemistry, 17(23), 2459, https://doi.org/10.1039/b702141k.

Lee, S.Y., Jin, S.H., Kim, S.M., Kim, J.W., 2016. Solution plasma process to synthesize silver nanofluids and their thermal conductivity behaviors. Metals and Materials International, 20(4), 695-699, https://doi.org/10.1007/s12540-014-4014-1.

Luo, Z., Wang, C., Wei, W., Xiao, G., Ni, M., 2014. Performance improvement of a nanofluid solar collector based on direct absorption collection (DAC) concepts. International Journal of Heat and Mass Transfer, 75, 262-271, https://doi.org/10.1016/j.ijheatmasstransfer.2014.03.072.

Mabey, T., Andrea Cristaldi, D., Oyston, P., Lymer, K.P., Stulz, E., Wilks, S., William Keevil, C., Zhang, X., 2019. Bacteria and nanosilver: the quest for optimal production. Crit Rev Biotechnol, 39(2), 272-287, https://doi.org/10.1080/07388551.2018.1555130.

Mallah, A.R., Kazi, S.N., Zubir, M.N.M., Badarudin, A., 2018. Blended morphologies of plasmonic nanofluids for direct absorption applications. Applied Energy, 229, 505-521, https://doi.org/10.1016/j.apenergy.2018.07.113.

Minardi, J.E., Chuang, H.N., 1975. Performance of a "black" liquid flat-plate solar collector. Solar Energy, 17(3), 179-183, https://doi.org/https://doi.org/10.1016/0038-092X(75)90057-2.

Modest, M., 2003. Radiative Heat transfer, 2nd Edition ed. Academic press, USA.

Nasrin, R., Parvin, S., Alim, M.A., 2015. Heat Transfer and Collector Efficiency through a Direct Absorption Solar Collector with Radiative Heat Flux Effect. Numerical Heat Transfer, Part A: Applications, 68(8), 887-907, https://doi.org/10.1080/10407782.2015.1023122.

Otanicar, T.P., Golden, J.S., 2009. Comparative Environmental and Economic Analysis of Conventional and Nanofluid Solar Hot Water Technologies. Environ Sci Technol, 43, 6032-6037.

Otanicar, T.P., Phelan, P.E., Golden, J.S., 2009. Optical properties of liquids for direct absorption solar thermal energy systems. Solar Energy, 83(7), 969-977, https://doi.org/10.1016/j.solener.2008.12.009.

Otanicar, T.P., Phelan, P.E., Prasher, R.S., Rosengarten, G., Taylor, R.A., 2010. Nanofluid-based direct absorption solar collector. Journal of Renewable and Sustainable Energy, 2(3), 033102, https://doi.org/10.1063/1.3429737.

Roh, J., Umh, H.N., Sung, H.K., Lee, B.-c., Kim, Y., 2012. Repression of photomediated morphological changes of silver nanoplates. Colloids and Surfaces A: Physicochemical and Engineering Aspects, 415, 449-453, https://doi.org/10.1016/j.colsurfa.2012.09.018.

Sharaf, O.Z., Rizk, N., Joshi, C.P., Abi Jaoudé, M., Al-Khateeb, A.N., Kyritsis, D.C., Abu-Nada, E., Martin, M.N., 2019. Ultrastable plasmonic nanofluids in optimized direct absorption solar collectors. Energy Conversion and Management, 199, https://doi.org/10.1016/j.enconman.2019.112010.

Sheffield Hallam University, 2019. Beer's Law. https://teaching.shu.ac.uk/hwb/chemistry/tutorials/molspec/beers1.htm. (Accessed 09 October 2019.

Tang, B., Xu, S., An, J., Zhao, B., Xu, W., 2009. Photoinduced Shape Conversion and Reconstruction of Silver Nanoprisms. J. Phys. Chem C, 113, 7025-7030.

Tang, B., Xu, S., Hou, X., Li, J., Sun, L., Xu, W., Wang, X., 2013. Shape evolution of silver nanoplates through heating and photoinduction. ACS Appl Mater Interfaces, 5(3), 646-653, https://doi.org/10.1021/am302072u.

Taylor, R.A., Hjerrild, N., Duhaini, N., Pickford, M., Mesgari, S., 2018. Stability testing of silver nanodisc suspensions for solar applications. Applied Surface Science, 455, 465-475, https://doi.org/10.1016/j.apsusc.2018.05.201.

Turkyilmazoglu, M., 2016. Performance of direct absorption solar collector with nanofluid mixture. Energy Conversion and Management, 114, 1-10, https://doi.org/10.1016/j.enconman.2016.02.003.

Tyagi, H., Phelan, P., Prasher, R., 2009. Predicted Efficiency of a Low-Temperature Nanofluid-Based Direct Absorption Solar Collector. Journal of Solar Energy Engineering, 131(4), 041004, https://doi.org/10.1115/1.3197562.

Walshe, J., Amarandei, G., Ahmed, H., McCormack, S., Doran, J., 2019. Development of poly-vinyl alcohol stabilized silver nanofluids for solar thermal applications. Solar Energy Materials and Solar Cells, 201, https://doi.org/10.1016/j.solmat.2019.110085.

Xu, G., Chen, W., Deng, S., Zhang, X., Zhao, S., 2015. Performance Evaluation of a Nanofluid-Based Direct Absorption Solar Collector with Parabolic Trough Concentrator. Nanomaterials, 5(4), 2131-2147, https://doi.org/10.3390/nano5042131.

Zhang, Q., Li, N., Goebl, J., Lu, Z., Yin, Y., 2011. A systematic study of the synthesis of silver nanoplates: is citrate a "magic" reagent? J Am Chem Soc, 133(46), 18931-18939, https://doi.org/10.1021/ja2080345.

Zmijan, R., Carboni, M., Capretto, L., Stulz, E., Zhang, X., 2014. In situ microspectroscopic monitoring within a microfluidic reactor. RSC Adv., 4(28), 14569-14572, https://doi.org/10.1039/c4ra01650e.

Supplementary information Unmarked-Revision

Click here to download Electronic Annex: SI Broadband paper Kimpton SE-D-20-01506 R1 Unmarked-Revision.docx

conflict of Interest Statement

Dr. Yanjun DAI
Editor, ***Solar Energy***

1st May 2020

Dear Dr. Dai,

Please find submitted an original research article, entitled “Silver nanofluids based broadband solar absorber through tuning nanosilver geometries”, by Harriet Kimpton, Eugen Stulz and Xunli Zhang for consideration for publication in *Solar Energy*. This manuscript has been neither published nor under consideration for publication elsewhere.

We have no conflicts of interest to disclose, but would like to acknowledge the funding provided by the University of Southampton.

If you require further information about this paper, please let us know anytime.

Sincerely,

Prof Xunli Zhang

University of Southampton